The Geometry of Fluid Membranes: Variational Principles, Symmetries and Conservation Laws

Jemal Guven and Pablo Vázquez-Montejo

Abstract The behavior of a lipid membrane on mesoscopic scales is captured unusually accurately by its geometrical degrees of freedom. Indeed, the membrane geometry is, very often, a direct reflection of the physical state of the membrane. In this chapter we will examine the intimate connection between the geometry and the physics of fluid membranes from a number of points of view. We begin with a review of the description of the surface geometry in terms of the metric and the extrinsic curvature, examining surface deformations in terms of the behavior of these two tensors. The shape equation describing membrane equilibrium is derived and the qualitative behavior of solutions described. We next look at the conservation laws implied by the Euclidean invariance of the energy, describing the remarkably simple relationship between the stress distributed in the membrane and its geometry. This relationship is used to examine membrane-mediated interactions. We show how this geometrical framework can be extended to accommodate constraints—both global and local—as well as additional material degrees of freedom coupling to the geometry. The conservation laws are applied to examine the response of an axially symmetric membrane to localized external forces and to characterize topologically nontrivial states. We wrap up by looking at the conformal invariance of the symmetric two-dimensional bending energy, and examine some of its consequences.

J. Guven (✉)
Instituto de Ciencias Nucleares, Universidad Nacional Autónoma de México,
Apdo. Postal 70-543, 04510 Mexico City, Mexico
e-mail: jemal@nucleares.unam.mx; jemalguven@gmail.com

P. Vázquez-Montejo
Facultad de Matemáticas, Universidad Autónoma de Yucatán, Periférico Norte,
Tablaje 13615, 97110 Mérida, Yucatán, Mexico

D.J. Steigmann (ed.), *The Role of Mechanics in the Study of Lipid Bilayers*,
CISM International Centre for Mechanical Sciences 577,
DOI 10.1007/978-3-319-56348-0_4

1 Introduction

Bilayers of amphiphilic molecules form the essential component of all cellular membranes, not only the plasma membrane enclosing the cell but also every membrane contained within it. Under physiological conditions, this bilayer is a fluid along the membrane; stretching is very costly, but it shears freely. By the 70s, it was beginning to become clear that on mesoscopic scales, which are often the scales that are most relevant physiologically and certainly the scales on which the global architecture comes into focus, the biochemical details of the membrane composition get telescoped into a small number of material parameters. Indeed, the membrane morphology itself is described surprisingly well by the geometrical degrees of freedom of a two-dimensional smooth surface. The membrane radius of curvature ($\sim$20 nm and up) is *large* compared to the bilayer thickness $\sim$5 nm. This is better than one could have hoped. While these surfaces may be smooth, they are rarely simple, reflecting the complex functions they play. To understand this morphological variety, it is necessary to possess the appropriate geometrical language. For the most part, this was understood by the mid-nineteenth century, to wit that two tensor fields characterize the surface geometry: the metric marking distances along the surface and the extrinsic curvature quantifying how it bends along different tangent directions. The two are not unrelated.

The physical behavior on mesoscopic scales is largely controlled by the bending energy of this surface, proportional to a quadratic in the membrane extrinsic curvature, Canham (1970); Helfrich (1973). For reviews, see Seifert and Lipowsky (1995); Bassereau et al. (2014); Tu and Ou-Yang (2014). Significantly, this energy depends only on the two fundamental tensors. What is more, modulo topology and boundary conditions, to an unusually good first approximation it is also unique.

Because the energy is determined completely by the geometry, the distribution of stress established along the membrane must *in turn* depend only on the geometry. This contrasts with the transverse distribution of stress across the membrane which does depend sensitively on the molecular details of the bilayer, as well as its interaction with water. But when we zoom out, these details contribute only to the constant of proportionality in the bending energy. The role they play is to set the rigidity. In this chapter, we review various aspects of the connection between the membrane geometry and the physics shaping it. Of course, almost always, additional agents need to be accommodated, and this direct connection gets modulated by the fields describing them.

We first examine how the bending energy, not necessarily in equilibrium, responds to deformations of the surface geometry (Sects. 2, 4). This turns on the behavior of the two fundamental tensors under deformation. The shape equation describing the surface geometry depends on the geometry through scalars constructed using these two tensors. We will develop in parallel the description of the surface in terms of its height above a plane. This representation is most useful when gradients in this function are small. This allows us to understand the local behavior consistent with membrane equilibrium.

The energy possesses symmetries: even if we disguise the fact by parametrizing the surface in terms of a height function, it is invariant under reparametrization—as any meaningful description of a physical theory should be; however, the effect of a tangential deformation of the surface is equivalent to a reparametrization of the surface except—and this is important—where the surface terminates; this apparently innocuous identification distinguishes the geometrical degrees of freedom from any additional material degrees of freedom overlaying the surface. And it has its physical consequences. Understanding how the metric and curvature behave under normal deformations of the surface permits us to describe not only its approach to equilibrium but also its behavior out of equilibrium.

The surface energy is obviously invariant under the Euclidean motions of its three-dimensional environment: translations and rotations. The bending energy of a symmetric fluid membrane is also scale invariant; this property of the two-dimensional bending energy distinguishes it from its one-dimensional counterpart, or for that matter from higher dimensional generalizations. If it were not for a constraint fixing the length, bending energy would tend to stretch a loop; a hypothetical three-dimensional surface would collapse. In two dimensions, the bending energy is independent of size. If this energy is isotropic, it turns out to be even invariant under the (angle preserving) conformal transformations of three-dimensional space, a property of two-dimensional surfaces that one could be forgiven for failing to anticipate (Sect. 7). In particular, it is invariant under inversion in spheres. Two different, indeed very different, geometries may possess identical bending energies. The energies may be identical but the local stresses supporting these geometries will generally be different.

Each symmetry implies a conservation law. In particular, the translational (rotational) invariance implies the existence of a conserved stress (torque) tensor, Capovilla and Guven (2002a) (see Sect. 5). It would not be an exaggeration to claim that the recognition of the role of symmetry has been central in the development of physics since the beginning of the 20$^{\text{th}}$ century. Improbable as it may appear from a traditional biophysical point of view, fluid membranes on mesoscopic scales are no exception; it could be argued that they provide a physical system par excellence supporting this claim.

In an unadorned fluid membrane, the identification of tangential deformations of the surface with reparametrizations implies constraints on the stresses associated with each term in the Hamiltonian, whether or not the membrane happens to be in equilibrium. We show how the stress tensor can be used to quantify the forces mediated by the membrane geometry. We also show how the conservation of the stress tensor permits direct access to the physics of axially symmetric shapes. Conformal invariance, happy accident or not, provides unexpected insight into the behavior of membranes well outside the regime where perturbation theory is reliable; even when the full symmetry is broken by constraints (Sect. 7).

Section 5 exploits extensively an adaptation of the calculus of variations introduced by one of the authors, Guven (2004). This approach, exploiting the structure equations describing the surface, provides a very direct construction of the stress tensor. Surprisingly, as we show, one does not need to know how the metric or the curvature respond to surface deformations to determine the approach to equilibrium. We show how this approach can be tweaked to accommodate local constraints on the geometry, and specifically a constraint on the metric. It also provides a natural framework in which to examine interactions mediated by the membrane as well as the boundary conditions on free edges. At the end of this section we present a complementary approach to the variational problem in which the equilibrium surface itself is treated as an emergent quantity from the two fundamental tensors. This approach exploits not the structure equations but the integrability conditions on these two tensors which follow from these equations. Unexpectedly, this approach provides a criterion for assessing membrane stability, Guven and Vázquez-Montejo (2013a). As we will attempt to communicate, each of the different approaches provides valuable insight into the underlying physics.

If the membrane consisted only of lipids, and they all responded in the same way, there would not be a lot to say. Intracellular membranes, however, display striking morphological diversity: contrast the spherical nuclear envelope punctured by pores with the endoplasmic reticulum (ER); or indeed the laminar stacks forming the rough ER with the tubular network forming its smooth counterpart. Then there are the flattened cisternae of the Golgi apparatus, as well as the convoluted inner membrane of a mitochondrion. And each membrane morphology is exquisitely adapted to its function. The downside is that life-threatening physiological malfunctions can all too often be traced to flaws in assembly.

What lends a membrane its specific morphology is the modulation of the behavior of the fluid bilayer by local or global constraints or biases, localized external forces, its composition and, as increasing recognized in recent years, its interactions with proteins or other macromolecules, themselves very often assembled into one or two-dimensional semi-flexible structures (for example, see Sens et al. 2008; Amoasii et al. 2013; Terasaki et al. 2013). Remarkably, on the scales that interest us, this additional structure is captured by fields or by some effective one or two-dimensional elastic structure interacting with the surface geometry. To understand how these interactions shape a membrane, it is invaluable to think in terms of the stresses they induce in the membrane. We will illustrate this point using a number of physiologically relevant but simple examples. We examine the forces constricting a membrane. We also examine the forces and torques, topological in origin, that sculpt the morphology of a toroidal vesicle, as well as the distribution of stress associated with them. Here nontrivial topology arises without the intervention of any exterior agent. These stresses are contrasted with their counterparts in a topologically spherical vesicle whose poles are pushed together by an external agency.

Before we begin, we need to introduce a few geometrical ideas on which the framework is built.

2 Surface Geometry: Intrinsic Versus Extrinsic Elements

We begin with a quick summary of a few essential geometrical concepts. This is not the place to present all of the details which would require a monograph in its own right. The interested reader can consult, Do Carmo (1976); Spivak (1999) or, for a less technical treatment, Kreyszig (1991). Some of this material is also covered nicely by Deserno in one of his excellent reviews (most recently, Deserno 2015). The reader may wish to glide over this section. It will, however, serve to establish notation and conventions.

We describe the surface parametrically in terms of a mapping into three-dimensional Euclidean space, $\Sigma : (u^1, u^2) \to \mathbf{X}(u^1, u^2)$, where u^1 and u^2 are *any* two local coordinates. Our description of Euclidean space will be Cartesian. The tangents to the coordinate curves associated with this parametrization form two surface tangent vectors at every point[1]: $\mathbf{e}_a = \partial_a \mathbf{X}$, $a = 1, 2$. These two vectors, in turn, define the surface (unit) normal vector $\mathbf{n}$. Now any vector field on the surface can be decomposed with respect to the basis vectors $\{\mathbf{e}_1, \mathbf{e}_2, \mathbf{n}\}$.

The two fundamental tensors: By the mid 19th century, it was already recognized that two surface tensor fields—constructed using derivatives of $\mathbf{X}$—describe the surface geometry completely. The first of these is the metric tensor induced on the surface from its Euclidean environment, whose components with respect to the parametrization are given by the Euclidean scalar product[2]

$$g_{ab} = \mathbf{e}_a \cdot \mathbf{e}_b \,. \tag{1}$$

If $ds^2 = d\mathbf{x} \cdot d\mathbf{x}$ is the line element in three-dimensional Euclidean space, its *pullback* to the surface is given by $ds^2\Big|_\Sigma = \mathbf{e}_a \cdot \mathbf{e}_b \, du^a du^b$. Thus g_{ab} quantifies distances between points on the surface and thus characterizes what we think of as its intrinsic geometry. In particular, the area element on the surface is given by $dA = \sqrt{g}\, du^1 du^2$, where $g = \det g_{ab} = |\mathbf{e}_1 \times \mathbf{e}_2|^2$.[3] If $g \neq 0$, g_{ab} has an inverse g^{ab}: $g^{ac} g_{cb} = \delta^a{}_b$. If Ψ is a scalar function on the surface, then $g^{ab} \partial_a \Psi \partial_b \Psi$ is another scalar. Indices are raised (lowered) using g^{ab} (g_{ab}). Let $\mathbf{V} = V^a \mathbf{e}_a$ be a surface vector field[4]; the metric allows us to associate a covector field V_a with V^a through the relationship, $V_a = g_{ab} V^b$.

---

[1] We abbreviate $\partial_a = \partial_a \mathbf{X} / \partial u^a$.

[2] We are interested specifically in surface tensors and the scalars constructed out of them. Consider a surface reparametrization $(u^1, u^2) \to (\bar{u}^1(u^1, u^2), \bar{u}^2(u^1, u^2))$. Define $J^{\bar{a}}{}_b = \partial \bar{u}^a / \partial u^b$, with inverse $J_{\bar{a}}{}^c : J^{\bar{a}}{}_c J_{\bar{b}}{}^c = \delta^{\bar{a}}{}_{\bar{b}}$. Tensor fields transform under reparametrization by matrix multiplication on each index with the Jacobian matrix of the reparametrization or its inverse. In particular, the metric transforms by $\bar{g}_{\bar{a}\bar{b}} = J_{\bar{a}}{}^c J_{\bar{b}}{}^d g_{cd}$. Note that the three Cartesian embedding functions $\mathbf{X} = (X^1, X^2, X^3)$ are each scalars under reparametrization: $\bar{X}^1(\bar{u}^1, \bar{u}^2) = X^1(u^1, u^2)$, etc.

[3] Under reparametrization, $\sqrt{\bar{g}} = \det J^{-1} \sqrt{g}$.

[4] It is simple to show that V^a transforms like a vector under reparametrization.

The covariant derivative ∇_a compatible with g_{ab} coincides with the projection onto the tangent directions of the derivative along the tangent curves, Do Carmo (1992). If $\mathbf{V} = V^a \mathbf{e}_a$, then its covariant derivative, a surface tensor, is given by

$$\nabla_a V^b = \mathbf{e}^b \cdot \partial_a \mathbf{V} = \partial_a V^b + \Gamma^b_{ac} V^c \,, \tag{2}$$

where $\Gamma^b_{ac} = \mathbf{e}^b \cdot \partial_a \mathbf{e}_c$ is symmetric in its lower indices by construction. It is straightforward to show that Γ^c_{ab} can be expressed entirely in terms of g_{ab} and its derivatives:

$$\Gamma^b_{ac} = \frac{1}{2} g^{bd} (\partial_a g_{cd} + \partial_c g_{ad} - \partial_d g_{ac}) \,, \tag{3}$$

identifying it, not coincidentally, with the Christoffel connection. The action of ∇_a on covectors as well as higher order tensor fields follow from the identification $\nabla_a \Psi = \partial_a \Psi$ on a scalar and the product (Leibnitz) formula for differentiation. Note that the identity $\nabla_a g_{bc} = 0$ follows.

An intrinsic measure of curvature is provided by the Riemann tensor, which quantifies the failure of covariant derivatives to commute. For a covector field V_a, the Ricci identity

$$(\nabla_a \nabla_b - \nabla_b \nabla_a) V_c = \mathcal{R}_{abc}{}^d \, V_d \,, \tag{4}$$

defines the Riemann tensor, $\mathcal{R}_{abc}{}^d$. It is constructed out of Γ^a_{bc} and its first derivatives, Do Carmo (1976).

In the familiar Monge representation, the surface is described in terms of its height $h(\mathbf{r})$ above a plane. If the plane is itself parametrized by Cartesian coordinates, $\mathbf{r} = x\,\mathbf{i} + y\,\mathbf{j}$, one has $\mathbf{e}_j = (\delta^1{}_j, \delta^2{}_j, \partial_j h)$, so that $g_{ij} = \delta_{ij} + \partial_i h \, \partial_j h$. Its inverse is given by

$$g^{ij} = \delta_{ij} - \frac{\partial_i h \partial_j h}{1 + |\nabla_0 h|^2} \,, \tag{5}$$

where $|\nabla_0 h|^2 = \partial_i h \partial_i h$. While $|\nabla h_0|^2$ is a scalar on the plane, it is not a surface scalar. The relevant scalar is $|\nabla h|^2 = g^{ab} \partial_a h \partial_b h$.

This representation of a surface has proven very useful when gradients are small (see, for example, Fournier 2007). With respect to an appropriate plane, it is always valid locally; even on complex geometries. However, it has its limitations, most notably if we attempt to access global information when the geometry is closed or its topology is nontrivial so that gradients necessarily not only become large but also diverge in places.

In this representation, $\sqrt{g} = \sqrt{1 + |\nabla_0 h|^2}$, so that the area is given by

$$A = \int d\mathbf{r} \, \sqrt{1 + |\nabla_0 h|^2} \,, \tag{6}$$

where we use the abbreviation $d\mathbf{r}$ to denote the area element on the base plane. The easiest way to see this is to note that the matrix g_{ij}, defined by Eq. (5) has eigenvalues

$1 + |\nabla_0 h|^2$ (corresponding to the eigenvector $\partial_i h$) and 1 (corresponding to a vector orthogonal on the plane to $\partial_i h$).

The second fundamental surface tensor is the extrinsic curvature, with components given by

$$K_{ab} = \mathbf{e}_a \cdot \partial_b \mathbf{n}\,; \tag{7}$$

it quantifies how fast the unit normal vector rotates into one tangent direction as one moves it along another. It thus captures the way that the surface curves in the Euclidean environment. This tensor is symmetric; as such, the linear map on tangent vectors $K^a{}_b = g^{ac} K_{cb}$ has two real eigenvalues, C_1 and C_2 (the principal curvatures). The surface curvature along a given direction $\mathbf{V}$ is given by $C(V) = V^a K_{ab} V^b$; it is extremal along the two corresponding orthogonal (principal) directions, along which it assumes the values C_1 and C_2. To see this, construct the constrained quadratic, $\mathcal{C}(V) = C(V) - \Lambda(V^a g_{ab} V^b - 1)$, where Λ is a Lagrange multiplier. Now $\mathcal{C}(V)$ is stationary when $K_{ab} V^b = \Lambda V_a$, or, equivalently, V^a is an eigenvector of $K^a{}_b$, with eigenvalue Λ. $C(V)$ is completely determined once we know the angle $\mathbf{V}$ makes with (one of) the principle two directions. This may be simple linear algebra but the geometrical consequences are far-reaching.

If the geometry is simple, it is possible to get along fine without knowing that curvature is a tensor; but good luck if it is not. The tensorial nature of K_{ab} will play an essential role in teasing out the relationship between stress and geometry. The two principal directions turn out to possess physical significance in the interpretation of the surface stress tensor.

An elementary calculation using height functions is useful to ground the definition of K_{ab}. If the base plane is tilted so as to coincide with the tangent plane to the surface at a given point, the curvature there is given by the Hessian of the height function: $K_{ij} = -\partial_i \partial_j h$. Its trace at this point (which we denote K) is given by $K = -\nabla_0^2 h$, where ∇_0^2 is the Laplacian defined on the base plane. Its determinant, correct to quadratic order,

$$\mathcal{K}_G = 2\det K_{ij} \approx (\nabla_0^2 h)^2 - (\nabla_i \nabla_j h)(\nabla_i \nabla_j h) = \nabla_i \left[\nabla_i h \nabla^2 h - \nabla_j h \, \nabla_i \nabla_j h\right] \tag{8}$$

is a divergence.

3 The Bending Energy

The bending energy of a homogeneous and isotropic fluid membrane is given by the Canham–Helfrich (CH) Hamiltonian, quadratic in the symmetric curvature invariants.These invariants can be constructed in terms of the trace $K = C_1 + C_2$, and the

determinant $\mathcal{K}_G = C_1\, C_2$ of $K^a{}_b = g^{ac} K_{cb}$,[5] so it reads, Canham (1970); Helfrich (1973); Evans (1974)

$$H_{CH}[\mathbf{X}] = \frac{1}{2}\,\kappa \int dA\,(K - C_0)^2 + \bar{\kappa} \int dA\,\mathcal{K}_G + \sigma A\,. \tag{9}$$

It involves two rigidity moduli, $\kappa \approx 20 k_B T$ and $\bar{\kappa}$. The constant spontaneous curvature C_0 reflects an asymmetry between the two sides of the bilayer; the parameter σ is interpreted either as a chemical potential or as a surface tension controlling the area A.[6] It is important to emphasize, despite the persistence of claims to the contrary, that σ is rarely the complete mechanical tension in the membrane. This issue will be addressed below. As Gauss famously was first to observe, the scalar $\mathcal{K}_G$ (known as Gaussian curvature) is invariant under isometry, depending only on the metric tensor. What is more, according to the Gauss–Bonnet theorem, the corresponding integrated energy is topological, modulo a boundary addition, Do Carmo (1976); Spivak (1999); on a closed single component membrane, it is irrelevant as far as determining the shape is concerned. We will see that it does not contribute explicitly to the stress. It does, however, play a role in determining the equilibrium geometry though its contribution to boundary conditions, or if the membrane is inhomogeneous. It is a mistake to ignore it.

The quadratic approximation: In terms of the height function, the quadratic approximation for the energy (9)—good when height gradients are small ($|\nabla h| \ll 1$)—reads

$$H \approx \frac{1}{2}\kappa \int d\mathbf{r}\,(\nabla_0^2 h)^2 + \frac{1}{2}\Sigma \int d\mathbf{r}\,(\nabla_0 h)^2 + \text{constant}\,, \tag{10}$$

where $\Sigma = \sigma + \kappa C_0^2/2$ is what we provisionally called surface tension augmented by spontaneous curvature, Lipowsky (2013). We saw that the term linear in K appearing in Eq. (9) is a divergence in this approximation, so it does not contribute to the local energy at this order. The constant $= \Sigma A_0$, proportional to the projected area, is usually ignored. It does, however, contribute to the stress in the membrane. Indeed, in the familiar textbook demonstration that σ is tension in a soap film, using a square frame with an adjustable edge, this is the only term appearing in H.

If one expands the energy in powers of gradients, the quartic term is negative. Note that

$$\sqrt{1 + |\nabla_0 h|^2} \approx 1 + \frac{1}{2}\,|\nabla_0 h|^2 - \frac{1}{8}|\nabla_0 h|^4 + \cdots\,. \tag{11}$$

[5] It is straightforward to confirm that the two remaining symmetric quadratics, $C_1^2 + C_2^2$ and $(C_1 - C_2)^2$, can be expressed as linear combinations of K^2 and $\mathcal{K}_G$.

[6] As we will show below, controlling area locally is equivalent, in equilibrium, to controlling it globally.

To our knowledge, all attempts to improve perturbatively on the quadratic approximation have failed. As we will show sometimes nature is obliging and small gradients can tell us a lot about the system. But more often, they are too restrictive and one needs to approach the problem non-perturbatively. For the moment, let us examine where they take us.

Linearized shape equation: The Euler–Lagrange (EL) or shape equation, describing the stationary shapes of the energy (10), is given to linear order by

$$(\nabla_0^2 - \lambda^2)\,\nabla_0^2 h = 0\,, \tag{12}$$

with a length scale $l = \lambda^{-1} = \sqrt{\kappa/\Sigma}$, indicating the scale below which bending rigidity dominates capillary forces: $l \approx 100\,\text{nm}$ for a typical fluid membrane. The derivation of Eq. (12) is a straightforward exercise in the calculus of variations.[7]

It is useful to slow down a moment and examine the elementary solutions of the linearized shape equation (12) in some detail. This will provide a guide as to what geometries we can expect to observe locally on a free membrane, as well as priming us to recognize behavior suggesting that some additional agent is involved.

Harmonic functions: Solutions of the linearized shape equation include minimal surfaces satisfying Laplace's equation on the plane, $\nabla_0^2 h = 0$. By the definition of curvature, these are symmetric saddles almost everywhere, with $K = 0$ or $C_1 = -C_2$. Typically, however, minimal surfaces are inconsistent with the boundary conditions—there are also no closed minimal surfaces—but they do feature prominently as local approximations of the physical geometry; sometimes they do even better, as we describe in the next paragraph. The Helmholtz equation, $(\nabla_0^2 - \lambda^2)\,h = 0$, also clearly provides solutions of the EL equation, with the same caveat. Any equilibrium surface can be described locally as a linear combination of solutions to the Laplace and Helmholtz equations.

Let us parametrize the plane in terms of the complex coordinate $Z = re^{i\varphi}$, where r and φ are polar coordinates; solutions of the two-dimensional Laplace equation are given by the real and imaginary parts of analytic functions $f(Z)$. Particular solutions are generated by $f(Z) = Z^n$, $n = 0, \pm 1, \pm 2, \ldots$; the dipole $n = 1$ describes a tilt; the quadrupole $n = 2$ describes a symmetric saddle, $n = 3, 4, \ldots$ describe monkey saddles and their many-tailed counterparts.

The monopole is generated by $f(Z) = \ln Z = \ln r + i\varphi$.

(1) The height function obtained from the real part is axially symmetric (the beginnings of a neck). The minimal surface spanning a large outer circular ring of radius R, and a small coaxial inner one raised above it by a height $h \ll R$ forms part of a catenoid. Indeed, the asymptotics of a catenoid reproduce the small gradient approximation.

(2) The imaginary part represents half of a helicoid, $h = p\,\varphi$, a spiral staircase or ramp (depending on the range of r).[8] Notice that while $\nabla_0^2 \varphi = 0, h = \varphi$ does describe

[7] For simplicity we will suppose that not only the surface height but also its normal vector are fixed on the boundary.

[8] The other half of helicoid is given by $h = c(\pi + \varphi)$.

an exact minimal surface. Curiously, this is the only (nonplanar) minimal surface described exactly by its linearization.[9] These two geometries, despite appearances, are symmetric saddle everywhere! Indeed, so also are the monkey saddles except at the origin. Notice that the Gaussian curvature on a monkey saddle vanishes at the origin. One can easily confirm that $\mathcal{K}_G$ is also axially symmetric in any one of these elementary geometries, wiggle as it may.

Minimal ramp and dipole: Let us examine, more closely, the ramp $h = p\,\varphi$ with inner radius r_0 extending out to some cutoff R_{cutoff}. Its pitch p provides a length scale. This is not an academic exercise because, recently, it was discovered that the sheets within the laminar stacks of the rough endoplasmic reticulum (ER) are connected by spiral ramps, Terasaki et al. (2013). However, a simple minimal ramp is costly energetically, with $E_{\text{ramp}} \sim p^2\sigma \ln R_{\text{Cutoff}}/r_0$; they also require a significant vertical force to hoist. Because its pitch is independent of r, its footprint does not decay as one moves away from the axis. Individual minimal ramps are thus inconsistent with planar stacking even if they are metrically flat ($\mathcal{K}_G \to 0$) far away.

One can, however, construct a ramp dipole by pairing parallel ramps with opposite chiralities: if the axes are separated by a distance $R > 2r_0$, the height function

$$\begin{aligned} h/p &= \text{Im}\ln[(Z - R/2)(\bar{Z} + R/2)] \\ &= \arctan[Rr\sin\varphi/(r^2 - R^2/4)] \end{aligned} \tag{15}$$

represents the dipole illustrated in Fig. 1a centered on the origin and aligned along the x-axis.

Here one observes the beauty of small gradients: superposition holds; if h_1 and h_2 are minimal, so is their sum.

The corresponding energy $E_{\text{dipole}} \sim p^2\sigma \ln R/r_0$ depends on the distance between axes; the pitch is now screened and the Gaussian curvature decays as $\mathcal{K}_G \sim -p^2R^2/r^6$ or faster, so the geometry rapidly becomes planar outside a core of size R.

Dipoles also stack much like a parking garage with the two ramps connecting parallel floors. It has been conjectured, Guven et al. (2014) that the basic element within the stacks of the rough ER is one of these dipoles. One still needs to explain what sets the distance between ramps, their pitch, their tilt, as well as the inner radius. Indeed, the sheets are not simple bilayers, but tetralayers consisting of a parallel pair of bilayers separated by a lumen; the inner boundaries are highly curved bilayers.

---

[9] Under a deformation $h(\mathbf{r}) \to h(\mathbf{r}) + \delta h(\mathbf{r})$, fixed on the boundary, the change in area A (6), is given by

$$\delta A = \int d\mathbf{r}\,\nabla_0 \cdot \mathbf{J}\,\delta h \tag{13}$$

where

$$\mathbf{J} = -\frac{\nabla_0 h}{(1 + |\nabla_0 h|^2)^{1/2}}\,, \tag{14}$$

so that $\nabla_0 \cdot \mathbf{J} = 0$ in equilibrium. One can evaluate $|\nabla_0 h|^2 = p^2/r^2$, so that $\mathbf{J} = p(-\sin\theta, \cos\theta)/r(1 + p^2/r^2)^{1/2}$ and $\nabla_0 \cdot \mathbf{J} = 0$.

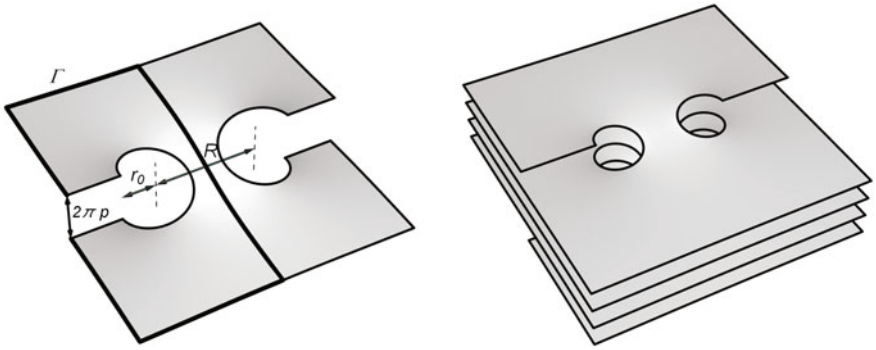

(a) Dipole (b) Ramp

Fig. 1 Ramp Dipole: **a** floor to floor and **b** stacked. The "square" contour Γ (heavy line) is used to determine the force between unpinned ramps, discussed in Sect. 5

In this chapter, the framework to address and answer some of these questions will be provided.

Biharmonic functions: Let us now examine solutions of the Biharmonic Equation $(\nabla^2)^2 h = 0$, describing the linearization of a membrane with $\Sigma = 0$. This is generally not true but we will see that there exist notable situations when it is. All solutions of $\nabla^2 h = 0$ are again solutions, as well as solutions with harmonic sources: $\nabla^2 h = J$, where $\nabla^2 J = 0$. Using the same method of complex variables used before, we look at harmonic sources in turn.

(1) For the constant function $J = 1$; $4\partial_Z \partial_{\bar{Z}} h = 1$, we find $h \sim |Z|^2$. This is the beginning of a sphere. Note that it is not analytic. Just as we did not possess the freedom to construct asymmetric saddles, this parabolic height function is axially symmetric.

(2) Next look at $J = \ln Z$. Now $4\partial_Z \partial_{\bar{Z}} h = \ln Z$ implies $h = |Z|^2(\ln Z - 1)$. This includes the singular axially symmetric surface $r^2 \ln r/r_0$ as well as the quadratically growing spiral $r^2\varphi$.[10] The surface $r^2 \ln r$ possesses a tangent plane at the origin. However, $\mathcal{K}_G$ diverges there. The parabolic appearance at the origin is deceiving. This is a danger of relying too heavily on visual cues. This curvature singularity signals the breakdown of the source-free equation indicating that a necessity of a distributional external force at the origin.

(3) One also find solutions $h \sim |Z|^2 Z^{\pm n}$. In particular, if $n = -2$, we have the hairpins $h = e^{-2i\varphi}$, illustrated in Fig. 2, wiggling with finite amplitude independent of r but with asymptotically decaying curvature. The curvature is again singular at the origin.

Helmholtz equation: If $\Sigma \neq 0$, then instead of the Biharmonic equation, we need to solve the Helmholtz equation. Its elementary solutions are given by $J = K_0(\lambda r)$, $K_n(\lambda r)\cos n\varphi$, $I_0(\lambda r)$, $I_n(\lambda r)\cos n\varphi$ (as well as the sines), where (i) K_n are modified

[10] Just as $\ln|\mathbf{r} - \mathbf{r}'|$ is proportional to the Green's function for the Laplacian, $-|\mathbf{r} - \mathbf{r}'|^2 \ln|\mathbf{r} - \mathbf{r}'|$ is its counterpart for the bilaplacian.

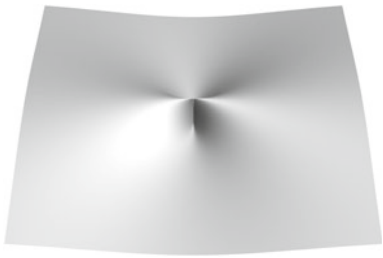

Fig. 2 Hairpin with $n = -2 : \cos 2\varphi$

Bessel functions diverging at the origin and monotonically decreasing as a function of r[11]; (ii) I_n are their monotonically increasing counterparts, diverging at infinity.

Now let $J = \nabla_0^2 h$. Then $h - J/\lambda^2$ satisfies Laplace's equation. Therefore there are no new solutions of Eq. (12) that are not already accounted for by forming linear combinations of harmonic functions and solutions of the Helmholtz equation.

Note that the axially symmetric function $K_0(\lambda r)$, the analogue of $-r^2 \ln r$, diverges at the origin. In this sense, it behaves like the harmonic $\ln r$.

One can check that there is an elementary Helmholtz spiral ramp, given by $K_0(\lambda r)\varphi$, forming a helix on its inner boundary, falling away remote from its axis.

Most general isotropic bending energy: The bending energy, (9), is not the only isotropic energy of interest. Energies involving curvature quartics have been introduced to explain periodic *egg carton* structures, Goetz and Helfrich (1996); Dommersnes and Fournier (2002); Manyuhina et al. (2010); accounting for the relative softness of gel phases may also involve a square root dependence on the curvature, not captured by a simple higher order symmetric polynomial, Diggins IV et al. (2015). All such extensions can be accommodated, without prejudice, by considering an energy of the general form,

$$H[\mathbf{X}] = \int dA\, \mathcal{H}\,(g_{ab}, K_{ab})\ , \tag{16}$$

where the energy density $\mathcal{H}$ (a scalar), is some given function (or functional, if derivatives are entertained) of the two fundamental tensor fields, g_{ab} and K_{ab}, defined earlier.

4 Beyond Height Functions: The Nonlinear Shape Equation

Let us now examine how the energy (16) changes in response to a deformation of the surface

$$\mathbf{X}(u^1, u^2) \to \mathbf{X}(u^1, u^2) + \delta\, \mathbf{X}(u^1, u^2)\,. \tag{17}$$

[11] The Green's function of the Helmholtz operator is proportional to $K_0(|\mathbf{r} - \mathbf{r}'|)$.

One way to do this is to first track the response of g_{ab} and K_{ab} to this deformation. To this end, it is instructive to decompose the deformation vector $\delta\mathbf{X}$ into tangential and normal parts,

$$\delta\mathbf{X} = \Phi^a\,\mathbf{e}_a + \Phi\,\mathbf{n}\,. \tag{18}$$

Clearly the two parts play very different roles.

Normal Deformations: The induced normal deformations are given by, Capovilla et al. (2003):

$$\delta_\perp g_{ab} = 2K_{ab}\Phi\,; \tag{19a}$$

$$\delta_\perp K_{ab} = -(\nabla_a\nabla_b - K_{ac}K^c{}_b)\Phi\,. \tag{19b}$$

The former provides a reinterpretation of curvature as the response of the metric to normal deformations; the latter reproduces the identification of the curvature with the Hessian of the height function ($h \approx \Phi$), when gradients are small and the reference geometry is planar so that the quadratic in K_{ab} vanishes.

The normal deformation also provides a generalization of the height function when the reference geometry is not a plane, valid whenever $\Phi << $ radius of curvature of this geometry. The curvature (19b) added to the surface standing at a height Φ is expressed in terms of the Hessian of Φ on the reference geometry screened (or anti-screened) by any pre-existing curvature.

Tangential deformations and reparametrizations: The tangential deformations of g_{ab} and K_{ab} are given by

$$\delta_\parallel g_{ab} = \nabla_a\Phi_b + \nabla_b\Phi_a\,; \tag{20a}$$

$$\delta_\parallel K_{ab} = (\nabla_c K_{ab} + K_{ac}\nabla_b + K_{bc}\nabla_a)\,\Phi^c\,. \tag{20b}$$

A mathematician may be aghast at the notation but should instantly recognize these two expressions as the Lie derivatives of the two tensors along the vector field defined by Φ^a. But this is not an accident: for the tangential deformations of a surface can be identified with the action of reparametrizations on the geometrical fields $\mathbf{X}$. Using the definition of the tangent vectors, the tangential deformation can be cast in the form $\delta_\parallel\mathbf{X} = \Phi^a\,\partial_a\mathbf{X}$, which is exactly how the embedding functions transform under an infinitesimal reparametrization of the surface, $u^a \to u^a - \Phi^a(u^1, u^2)$. The expressions for $\delta_\parallel g_{ab}$ and $\delta_\parallel K_{ab}$ thus should describe how the metric and any symmetric covariant tensor transform under this reparametrization: and this is by a Lie derivative. They are completely determined by the tensorial character of these variables; the details of their construction in terms of $\mathbf{X}$ are irrelevant. In this context, it should be noted that $\delta_\parallel K_{ab}$ or, for that matter, $\delta_\parallel$ of any surface tensor constructed from $\mathbf{X}$ does not depend on the metric: one can confirm that (and ditto for g_{ab} with the obvious replacement)

$$\delta_\parallel K_{ab} = (\partial_c K_{ab} + K_{ac}\partial_b + K_{bc}\partial_a)\,\Phi^c\,. \tag{21}$$

Using these results, it only takes a short step to see that the tangential deformation of any energy of the form (16) is given by the integral of a divergence. We first recall that, given any symmetric matrix B_{ab} (and, in particular, g_{ab}), $\partial\sqrt{\det B}/\partial B_{ab} = \sqrt{\det B}\, B^{-1ab}/2$. It then follows that, when the metric is varied, the area measure changes by

$$\delta\, dA = \frac{1}{2} dA\, g^{ab}\delta g_{ab}\,. \tag{22}$$

Using Eq. (20a), we have $g^{ab}\delta_\parallel g_{ab} = \nabla_a \Phi^a$[12], so that $\delta_\parallel dA = dA\, \nabla_a \Phi^a$; in addition, because $\mathcal{H}$ is a scalar depending only on $\mathbf{X}$, $\delta_\parallel \mathcal{H} = \nabla_a \mathcal{H}\, \Phi^a$. Summing terms, we find that any energy of the form (16) changes by a divergence

$$\delta_\parallel H = \int dA\, \nabla_a(\mathcal{H}\, \Phi^a)\,. \tag{23}$$

Using Stoke's theorem, the rhs can be cast as a boundary term $\oint ds\, \mathcal{H}\, l_a \Phi^a$ or equivalently $\oint ds\, \mathcal{H}\mathbf{l}\cdot\delta\mathbf{X}$, so that it makes no contribution to the response in the bulk and vanishes if the surface is closed. Here $l_a = g_{ab}l^b$ are the covariant components of $\mathbf{l} = l^a\mathbf{e}_a$, the surface tangent normal to its boundary (its conormal) pointing out of the surface. The upshot is that tangential deformations of the surface can be discounted everywhere except on boundaries where new surface is generated. Boundaries do get pushed about and, as Eq. (23) indicates, tangential deformations will play a role in understanding the behavior on them. There is a physically important corollary of the reparametrization invariance of the energy Eq. (16) and the identification of tangential deformations with reparametrizations: Because the tangential deformation is given by Eq. (23), derivatives of tangential surface deformations never occur as boundary terms. Nor can they arise when boundary energies are accommodated. Caveat: if there is a local constraint on the surface deformation, $\delta\mathbf{X}$, such as isometry, one needs to be more circumspect vis a vis the independence of Φ and Φ^a; for tangential deformations will tag along with their normal counterparts. Specifically, the constraint $\delta g_{ab} = 0$ is equivalent to

$$\nabla_a \Phi_b + \nabla_b \Phi_a + 2K_{ab}\Phi = 0\,. \tag{24}$$

The Gauss–Weingarten equations: The derivations of Eqs. (19) and (20a) are simplified significantly using the structure equations that capture the connection between intrinsic and extrinsic geometry:

$$\nabla_a \mathbf{e}_b = -K_{ab}\,\mathbf{n}\,; \tag{25a}$$

$$\partial_a \mathbf{n} = K_a{}^b\,\mathbf{e}_b\,. \tag{25b}$$

[12] $\nabla_a \Phi^a = \partial_a(\sqrt{g}\Phi^a)/\sqrt{g}$.

The Weingarten equation (25b) captures directly the definition of K_{ab} (7). If Eq. (25a) appears mysterious, note that $\partial_a \mathbf{e}_b$, while not itself a surface tensor (or, more correctly, a triplet of tensors) may be expanded with respect to the basis vectors:

$$\partial_a \mathbf{e}_b = \Gamma^c_{ab} \mathbf{e}_c - K_{ab}\, \mathbf{n}\,. \tag{26}$$

One finds that $\Gamma^c_{ab} = \mathbf{e}^c \cdot \partial_a \mathbf{e}_b$ is the Christoffel connection (3) constructed using g_{ab}. While neither $\partial_a \mathbf{e}_b$ nor $\Gamma^c_{ab} \mathbf{e}_c$ is a tensor, their difference $\nabla_a \mathbf{e}_b$ is. And ∇_a is the covariant derivative introduced in Eq. (2).

To illustrate the utility of these equations, let us go back and derive Eqs. (19). Using the definition of g_{ab} (1) we have

$$\begin{aligned} \delta_\perp g_{ab} &= \mathbf{e}_a \cdot \partial_b(\Phi \mathbf{n}) + (a \leftrightarrow b) \\ &= \mathbf{e}_b \cdot \partial_b \mathbf{n}\ \Phi + (a \leftrightarrow b) \\ &= 2K_{ab}\, \Phi\,, \end{aligned} \tag{27}$$

where we use Eq. (25b) on the last line. On the other hand, to determine $\delta_\perp K_{ab}$, we require an intermediate result which follows from the orthogonality of $\mathbf{n}$ to the surface: $\mathbf{e}_a \cdot \mathbf{n} = 0$ and $\mathbf{n}^2 = 1$ together imply $\delta_\perp \mathbf{n} = -\partial_b \Phi\, \mathbf{e}^b$. Now using the definition of K_{ab}, given by Eq. (7), we have

$$\begin{aligned} \delta_\perp K_{ab} &= \mathbf{e}_a \cdot \partial_b(\delta_\perp \mathbf{n}) + \partial_a(\mathbf{n}\Phi) \cdot K_b{}^c \mathbf{e}_c \\ &= -\nabla_a \nabla_b\, \Phi + K_{ac} K^c{}_b \Phi\,. \end{aligned} \tag{28}$$

The Gauss–Codazzi and Codazzi–Mainardi equations: It is clear that the tensors g_{ab} and K_{ab} are not independent. Even naively the counting is wrong. Their interdependence is quantified by the Gauss–Codazzi (GM) and Codazzi-Mainardi (CM) equations, given by

$$\mathcal{R} = K^2 - K_{ab} K^{ab}\,; \tag{29a}$$

$$\nabla^b \left(K g_{ab} - K_{ab}\right) = 0\,, \tag{29b}$$

where $\mathcal{R}$ is the scalar curvature (defined in a moment). These three equations arise as integrability conditions on Eq. (25a). This is easy to show. Rewrite Eq. (25a) as $\mathbf{G}_{ab} = \nabla_a \mathbf{e}_b + K_{ab}\, \mathbf{n} = 0$. Now $\nabla_a \mathbf{G}_{bc} - \nabla_b \mathbf{G}_{ac} = 0$, or

$$[\nabla_a, \nabla_b]\, \mathbf{e}_c = \nabla_a (K_{bc} \mathbf{n}) - \nabla_b (K_{ac} \mathbf{n})\,. \tag{30}$$

Whereas

$$[\nabla_a, \nabla_b]\, \mathbf{e}_c = R_{abc}{}^d\, \mathbf{e}_d \tag{31}$$

as a consequence of the Ricci identities (4),

$$\nabla_a(K_{bc}\mathbf{n}) - \nabla_b(K_{ac}\mathbf{n}) = (\nabla_a K_{bc} - \nabla_b K_{ac})\,\mathbf{n} + (K_{ac}K_{bd} - K_{ad}K_{bc})\,\mathbf{e}^d \tag{32}$$

on account of Eq. (25b). Equating tangential and normal terms implies

$$\mathcal{R}_{abcd} - K_{ac}K_{bd} + K_{ad}K_{bc} = 0\,; \tag{33a}$$

$$\nabla_a K_{bc} - \nabla_b K_{ac} = 0\,. \tag{33b}$$

The first set of equations tells us that the (intrinsic) Riemann tensor induced on a surface embedded in Euclidean space is determined completely by the extrinsic curvature tensor. The second set of equations is a covariant statement of the fact that the extrinsic curvature is a Hessian.

Note that there are counterparts of the integrability conditions on the Weingarten equation (25b) but they provide no additional constraint, simply reproducing Eq. (33b).

For a two-dimensional geometry these equations simplify. It is easy to see that the Riemann tensor has a single independent component, say R_{1212}.[13] As a result, it is completely captured by the scalar $\mathcal{R}$:

$$\mathcal{R}_{abcd} = (g_{ac}g_{bd} - g_{ad}g_{bc})\mathcal{R}/2\,. \tag{35}$$

Equation (29a) follow on contraction. In addition, it is clear that there are only two independent Codazzi-Mainardi equations (33b) on a two-dimensional surface: $\nabla_1 K_{21} - \nabla_2 K_{11} = 0$ and $\nabla_1 K_{22} - \nabla_2 K_{12} = 0$. These two equations are equivalent to the contracted Codazzi- Mainardi equations. For two-dimensional surfaces, there are three integrability conditions.

The GC equation (29a) indicates that the Gaussian curvature is also an isometry invariant, depending as it does only on the metric: $2\mathcal{K}_G = \mathcal{R}$.[14] This is the content of Gauss's Theorema egregium. The CM equations (29b) is the statement that the tensor $K_{ab} - K\,g_{ab}$ is covariantly conserved, an identity that is very useful to recall when taking covariant derivatives of the extrinsic curvature.

Normal deformations and energy: We have looked at the response of the energy to tangential deformations. Let us now track its response to a normal deformation—one that pushes the surface outwards. Consider, to get started, the energy proportional to the area, $H = \sigma A$, describing any interface. Using Eqs. (19) and (22) we have

[13] Note that the Ricci identify (4) implies $R_{abcd} = -R_{bacd}$; whereas its application to the metric tensor implies $R_{abcd} = -R_{abdc}$:

$$0 = [\nabla_a, \nabla_b]g_{cd} = R_{abcd} + R_{abdc}\,. \tag{34}$$

These account for all the independent constraints on R_{abcd} on a two-dimensional surface.

[14] The identity $\det K^a{}_b = (K^2 - K_{ab}K^{ab})/2$ is true for the determinant of any two-dimensional symmetric matrix.

$$\delta_\perp A = \int dA\, K \Phi\,. \tag{36}$$

As a consequence, H is stationary for fixed boundaries when $K = 0$, representing a minimal surface or $\mathbf{n} \cdot \nabla^2 \mathbf{X} = 0$ where the Laplacian appearing here is the Laplacian on the surface constructed using g_{ab}. This is the nonlinear counterpart of Laplace's equation on the plane presented earlier. Note that the three Cartesian coordinates satisfy the Laplace equation, or $\nabla^2 \mathbf{X} = 0$. This is because the contracted Gauss equation (25a) implies that the tangential projections vanish identically, or $\mathbf{e_a} \cdot \nabla^2 \mathbf{X} = 0$.

Now look at $H_B = \frac{1}{2}\kappa \int dA\, K^2$. Using the definition $K = g^{ab} K_{ab}$, as well as the general identity for matrix inverses, $\delta g^{ab} = -g^{ac} g^{bd} \delta g_{ab}$, Eq. (19) now imply:

$$\delta_\perp K = -(\nabla^2 + K_{ab} K^{ab})\Phi\,. \tag{37}$$

As a consequence:

$$\delta_\perp H_B = \kappa \int dA[-K(\nabla^2 + K_{ab} K^{ab}) + K^3/2]\Phi\,. \tag{38}$$

One may now use Stoke's theorem to perform two integrations by parts to peel derivatives appearing in the Laplacian off Φ and transfer them to K. Applying identical reasoning to the term linear in K appearing in the CH energy (9), the shape equation describing equilibrium membrane states in the absence of external forces is given by Capovilla and Guven (2002b)

$$\mathcal{E} = -\kappa \nabla^2 K + 2\kappa K \left(\mathcal{K}_G - K^2/4\right) - 2\kappa\, C_0\, \mathcal{K}_G + \Sigma\, K = 0\,. \tag{39}$$

In the presence of a pressure difference P across the surface, the surface geometry satisfies the equation: $\mathcal{E} = P$. This is a consequence of the intuitively simple identity

$$\delta_\perp V = \int dA\, \Phi\,. \tag{40}$$

The change in volume is the base area by the height! Thus, an energy contribution of the form $-PV$ has normal EL derivative $-P$.

Early derivations of Eq. (39), notably in Refs. Ou-Yang and Helfrich (1987, 1989), tended not to exploit the fundamental tensors explicitly. Notice the cubic nonlinearity in the curvature appearing in Eq. (39); it has its source in the term quadratic in curvature appearing in $\delta_\perp K_{ab}$. It is simple to confirm that the linearization of Eq. (39) with respect to a planar reference plane reproduces Eq. (12).

A comment on height functions: Let us reexamine the variational principle in the Monge representation. We saw that, under a deformation $h(\mathbf{r}) \to h(\mathbf{r}) + \delta h(\mathbf{r})$, the change in area A (6), is given by Eq. (9). h is a scalar field, both on the base and on the surface, so it should be possible to express the rhs of Eq. (9) in a manifestly

covariant form. Recall that, while $|\nabla_0 h|^2$ is a scalar on the reference plane, it is not a surface scalar. In fact, the density $\sqrt{g}$ is constructed in this parametrization in terms of $|\nabla_0 h|^2$.

The EL derivative of A appearing in Eq. (9) is clearly a divergence on the base plane. While not obvious, it should also be a divergence on the surface. If we use the identity $g^{ij}\partial_j h = \partial_i h/(1+|\nabla_0 h|^2) = \partial_i h/g$, we see that

$$\partial_i \left(\frac{\partial_i h}{(1+|\nabla_0 h|^2)^{1/2}} \right) = \partial_i (\sqrt{g} g^{ij} \partial_j h) = \sqrt{g} \nabla^2 h \,, \tag{41}$$

so that we can express δA in the manifestly reparametrization invariant form:

$$\delta A = -\int dA \, \nabla^2 h \, \delta h \,. \tag{42}$$

The Laplacian ∇^2 ($= g^{ab}\nabla_a \nabla_b$) is the Laplacian on the surface, not the base plane. One does not need to abandon surface reparametrization invariance when height functions are used. However note that $|\nabla h|^2 = |\nabla_0 h|^2/g$ or $g = 1/(1-|\nabla h|^2)$. Scalars do get conflated with densities.

In the Monge representation, $\mathbf{n} = (-\partial_i h, 1)/\sqrt{g}$, so that projecting (25a) onto the vertical $\mathbf{k}$, we identify

$$K_{ij}/\sqrt{g} = -\nabla_i \nabla_j h \,, \tag{43}$$

where ∇_i is the surface covariant derivative. Thus $K = -\sqrt{g}\nabla^2 h$.

Projecting Eq. (26) onto the Cartesian directions on the plane, one also finds that $\Gamma^k_{ij} = K_{ij}\nabla_k h/\sqrt{g}$; the connection is proportional to the extrinsic curvature. In the Monge representation the concepts of intrinsic and extrinsic geometry also get conflated.

Anisotropic energies: Other contributors discuss anisotropies. Consider the replacement of the bending energy Eq. (9) by an expression of the more general form

$$H = \int dA \, \mathcal{H}(C_1, C_2) \,, \tag{44}$$

say $\mathcal{H} = \kappa(C_1^2 + \alpha C_2^2)/2$, where $\alpha \neq 1$. It is convenient to know how C_1 and C_2 transform. One has $C_I = V_I^a K_{ab} V_I^b$, so that $\delta_\perp C_I = V_I^a V_I^b \delta_\perp K_{ab}$—an equation familiar in quantum mechanics as the first order perturbation in the eigenvalue due to a perturbation in the Hamiltonian. Now using Eq. (19b), we discover

$$\delta_\perp C_I = -V_I^a V_I^b \nabla_a \nabla_b \Phi + C_I^2 \Phi \,. \tag{45}$$

The peeling process can be performed exactly as before. Now, however, derivatives of the principal vector fields will appear in the first variation. On a surface only two scalars can be constructed using derivatives of a unit vector field, V^a: its divergence $I_1 = \nabla_a V^a$ and its curl, $I_2 = \epsilon^{ab}\nabla_a V_b$ (ϵ^{ab} is the antisymmetric

Levi–Cita tensor). Using the identity $\epsilon^{ab} = V^a V_\perp^b - V_\perp^a V^b$,[15] we find $I_2 = -V_\perp^a V^b \nabla_b V_a$, which is identified as the geodesic curvature along the integral curves of the vector field V^a.

The derivation of the shape equation presented in this section highlights the geometry. It is also perfectly adequate if one is interested in identifying membrane shapes. But it still has its limitations: for we are not only interested in shapes; indeed two very different models may predict qualitatively identical shapes. How then do we discriminate between them? What is missing is the distribution of stress underpinning the geometry, without which access to the forces acting on the membrane or transmitted by it is limited. This is simple enough, using a minimum of geometry, if gradients are small or the geometry is axially symmetric. We will have more to say about this approach. But we will now show that the little geometry we have introduced suggests a better way. We will also see there is a remarkably simple connection between the bending stress (as well as the torques) and the surface geometry, a consequence of the fact that the energy depends only on the geometry.

5 Stress and Geometry

The surface energy is invariant with respect to spatial translations. Using Noether's theorem, we know that this invariance implies the existence of a conserved current, identified as the stress tensor. This can be constructed by reassembling the normal and tangential boundary contributions to the energy associated with a translation. This was first done in Capovilla and Guven (2002b) (and even earlier in a relativistic context, in Arreaga et al. 2000).[16] The approach we describe here involves a refinement of the derivation in Capovilla and Guven (2002b), introduced a few years later by one of the authors, Guven (2004). There is no need to decompose deformations into normal and tangential parts; at the end of the calculation we will, however, interpret the conservation law by examining its projections.

We have seen that the energy (16) depends implicitly on the shape $\mathbf{X}$ through the two fundamental tensors. Thus far we have not fully exploited this dependence. While the metric and the extrinsic curvature are not independent, it is possible to treat them as though they were by making use of the method of Lagrange multipliers to record the steps in their construction in terms of $\mathbf{X}$ as local constraints and reformulating an unconstrained problem in the calculus of variations as a locally constrained one. We do this by replacing the energy H by the functional $H_C = H_C[\mathbf{X}, \mathbf{e}_a, \mathbf{n}, g_{ab}, K_{ab}, \mathbf{f}^a, f^a, f^n, T^{ab}, H^{ab}]$, defined by

[15] $V_\perp^a = \epsilon^{ab} V_b$ is orthogonal to V^a.

[16] A later derivation accommodating the finite thickness of the membrane is presented in Lomholt and Miao (2006).

$$H_C = H[g_{ab}, K_{ab}] + \int dA\, \mathbf{f}^a \cdot (\mathbf{e}_a - \partial_a \mathbf{X}) - \int dA\, f^a\, \mathbf{e}_a \cdot \mathbf{n} + \frac{1}{2}\int dA\, f^n(\mathbf{n}\cdot\mathbf{n} - 1) + \frac{1}{2}\int dA\, T^{ab}(g_{ab} - \mathbf{e}_a \cdot \mathbf{e}_b) - \int dA\, H^{ab}(K_{ab} - \mathbf{e}_a \cdot \partial_b \mathbf{n})\,. \quad (46)$$

While it does appear that we have just taken a step in the wrong direction, this is not the case. Bear with us! We are now freed to treat H itself as a functional of two independent tensor fields, rather than of the embedding functions, i.e., $H[g_{ab}, K_{ab}]$. The construction of g_{ab} and K_{ab}, consigned to the constraints, is clearly independent of the specific choice of H.[17]

There is also an element of flexibility in this construction: we choose to introduce the tangent and normal vectors ($\mathbf{e}_a$ and $\mathbf{n}$), mediating the construction of g_{ab} and K_{ab} in terms of $\mathbf{X}$, as independent fields. As will be evident in a moment there is a good reason for doing this.

The tensorial character of the Lagrange multipliers reflects the constraint they enforce: $\mathbf{f}^a$, appearing in Eq. (46), is associated with the identification of $\mathbf{e}_a$ as the two tangent vectors adapted to the parametrization; f^a is associated with the implicit identification of the normal vector and f^n enforces its normalization. The fields T^{ab} and H^{ab}, completing the identification of g_{ab} and K_{ab} as the two fundamental tensors, are symmetric tensors.

It is now legitimate to vary independently each of the geometric fields $\mathbf{X}$, $\mathbf{e}_a$, $\mathbf{n}$, g_{ab} and K_{ab}. We will perform the variations in this same order. The first three of these fields appear only in the constraints, so their variations can be performed without reference to H. Significantly, the embedding functions appear only in the tangency constraint, imposed by the multiplier fields, $\mathbf{f}^a$. The translational invariance of the energy is captured by the fact that $\mathbf{X}$ also appears only through its derivative. One determines, almost trivially, the response of H_C to a deformation $\delta\mathbf{X}$:

$$\delta_{\mathbf{X}} H_C = -\int dA\, \mathbf{f}^a \cdot \partial_a \delta\mathbf{X}\,. \quad (47)$$

An integration by parts is now used to peel the derivative off the variation; the EL derivative with respect to $\mathbf{X}$ is then identified as a divergence:

$$\frac{\delta H_C}{\delta \mathbf{X}} = \frac{1}{\sqrt{g}}\,\partial_a\left(\sqrt{g}\,\mathbf{f}^a\right) = \nabla_a \mathbf{f}^a\,. \quad (48)$$

Thus, in equilibrium,

$$\nabla_a \mathbf{f}^a = 0\,, \quad (49)$$

[17] In this approach, the deformation vector $\delta\mathbf{X}$ is never disassembled into normal and tangential parts, so that its reassembly is never necessary.

or $\mathbf{f}^a$ is conserved. Below, this tensor will be identified as the stress. We will be interested in the force per unit length transmitted across curves on the surface, given by the projection $\mathbf{f}_\perp := l_a \mathbf{f}^a$, where $\mathbf{l} = l^a \mathbf{e}_a$ is the conormal, introduced below Eq. (23).[18]

The EL equations for $\mathbf{e}_a$ and $\mathbf{n}$ identify the tangential and normal projections of $\mathbf{f}^a$ completely in terms of the two tensor-valued multipliers, T^{ab} and H^{ab}:

$$\mathbf{f}^a = f^{ab}\mathbf{e}_b + f^a \mathbf{n}\,, \tag{50}$$

where

$$f^{ab} = T^{ab} - H^{ac}K_c{}^b\,, \quad f^a = -\nabla_b H^{ab}\,. \tag{51}$$

The EL equations for g_{ab} and K_{ab} determine T^{ab} and H^{ab} in terms of the Euler–Lagrange derivatives of the energy density $\mathcal{H}$ with respect to g_{ab} and K_{ab}:

$$T^{ab} = -\frac{2}{\sqrt{g}}\frac{\delta(\sqrt{g}\mathcal{H})}{\delta g_{ab}}\,; \quad H^{ab} = \frac{\delta \mathcal{H}}{\delta K_{ab}}\,. \tag{52}$$

This completes the construction of $\mathbf{f}^a$. The normalization and sign of T^{ab} are chosen so that this tensor coincides with the metric stress tensor (see, for example, Wald 2010). However, unless $\mathcal{H}$ is independent of K_{ab} (so that $H^{ab} = 0$), T^{ab} is not the complete stress. Nor is it conserved.

The structure captured in Eqs. (51) and (52) is independent of the specific form of H. As promised, the stress is completely determined by the geometry. This is quite unlike the familiar situation in continuum mechanics where in-plane static shear—which is not supported by a two-dimensional incompressible fluid—generates stress.

Now let H be the CH energy given by Eq. (9). One then identifies, Capovilla and Guven (2002b); Guven (2004)

$$\mathbf{f}^a = \left[\kappa\,(K - C_0)\left(K^{ab} - \frac{1}{2}(K - C_0)g^{ab}\right) - \sigma g^{ab}\right]\mathbf{e}_b - \kappa\,\nabla^a K\,\mathbf{n}\,. \tag{53}$$

To confirm this, note that $\mathcal{H}$ involves a sum of terms proportional to $\mathcal{H}_n = K^n/n$, $n = 0, 1, 2$. For each n, straightforward calculus gives for the corresponding tensors defined by Eq. (52), $T_n^{ab} = K^{n-1}\left(2K^{ab} - K g^{ab}/n\right)$ and $H_n^{ab} = K^{n-1}g^{ab}$, so that the contribution to the stress (51) is

$$\mathbf{f}_n^a = K^{n-1}(K^{ab} - K g^{ab}/n)\,\mathbf{e}_b - \nabla^a K^{n-1}\,\mathbf{n}\,. \tag{54}$$

The Gaussian energy is not of this form. However, one can use the identity $\mathcal{K}_G = (K^2 - K_{ab}K^{ab})/2$ to show that $T_G^{ab} = K K^{ab} - K^{ac}K_c{}^b$, and $H_G^{ab} = K g^{ab} - K^{ab}$. As a result, the tangential stress, $T^{ab} - H^{ac}K_c{}^b$, appearing in Eq. (51) vanishes identically; its normal counterpart vanishes on account of the CM equations, (29b).

[18] If $\mathbf{t} = t^a \mathbf{e}_a$ is the unit tangent vector to the curve, $\mathbf{l}\cdot\mathbf{t} = 0$ or $g_{ab}l^a t^b = 0$ or $l_a t^a = 0$.

The upshot is that there is no Gaussian stress, and the Gaussian modulus $\bar{\kappa}$ does not feature in $\mathbf{f}^a$, a reflection of the topological nature of this energy.

In the case of an interface or a soap film, described by an energy proportional to area, $H = \sigma A$, the stress is tangential with $f^{ab} = -\sigma\, g^{ab}$ and $f^a = 0$. The proportionality to g^{ab} indicates that the tangential stress is isotropic; it is also homogeneous because σ is constant.

The stress in a fluid membrane is quadratic in curvature; as a consequence the stress is generally neither homogeneous nor isotropic. We note, however, that the tangential stress f^{ab} is a polynomial in K^{ab} and g^{ab}; this implies that the orthogonal eigenvectors of K^{ab}, $\mathbf{V}_1$ and $\mathbf{V}_2$, are also eigenvectors of f^{ab}. For pure bending (with $C_0 = 0$, $\sigma = 0$), the eigenvalues of f^{ab} are now easily identified as $f_1 = \kappa\,(C_1^2 - C_2^2)/2 = -f_2$. The tangential bending stress therefore is bounded by f_1 and f_2 which it assumes along these directions. If $C_1 < C_2$, then the membrane is under tension along $\mathbf{V}_1$, and under an equal compression along the orthogonal direction, $\mathbf{V}_2$. Because $f_1 + f_2 = g_{ab} f^{ab} = 0$, this is equivalent to the statement that the tangential bending stress is traceless. This is also not an accident. It can be understood to be a consequence of the scale invariance of the two-dimensional bending energy. Indeed, invariance of the bending energy under a rescaling $\delta\mathbf{X} = \lambda\mathbf{X}$ implies $f^a{}_a = 0$, Capovilla and Guven (2002b); Guven (2005). This is very different from the behavior we observe in an interface where the stress is tensile everywhere. More generally, let H be scale invariant. Equation (47) then implies that the contribution to δH due to $\mathbf{X}$ is proportional to

$$\int dA\, \mathbf{f}^a \cdot \nabla_a \mathbf{X} = \int dA\, f^a{}_a = 0\,, \tag{55}$$

and, for energy densities of the form $\mathcal{H}(g_{ab}, K_{ab})$, there are no boundary additions (these will be discussed below). As a consequence $f^a{}_a = 0$ pointwise. If, however, the energy involves higher derivatives of either g_{ab} or K_{ab}, boundary additions may show up, implying that the trace does not necessarily vanish but is a divergence: $f^a{}_a = \nabla_a g^a$, where g^a is some vector field. A scale invariant energy with this property is easy to construct, given by $\int dA\, \sqrt{\nabla_a K \nabla^a K}$, but without any physical application that we are aware of. For the curious, we remark that one needs to look at energies in higher dimensions involving derivatives to encounter polynomial examples displaying a $g^a \neq 0$.

Notice also that the bending stress vanishes on minimal surfaces, with $K = C_1 + C_2 = 0$, and on spheres, with $C_1 = C_2$. Normal stress is not supported in either case, for this requires nonvanishing gradients in K. On any other surface, the bending stress may change from tension to compression along a given direction. In fact, the integrated force may vanish but the torque need not. We will encounter this behavior in toroidal vesicles.

The force per unit length $\mathbf{f}_\perp$ transmitted across any curve can be expanded with respect to the orthonormal basis, $\{\mathbf{t}, \mathbf{l}, \mathbf{n}\}$, adapted to the curve, $\mathbf{f}_\perp = f_{\perp\perp}\mathbf{l} + f_{\perp\parallel}\mathbf{t} + f_\perp \mathbf{n}$, where we introduce the notation, $A_{\perp\perp} := l^a l^b A_{ab}$, $A_{\perp\parallel} := l^a t^b A_{ab}$, and

$A_{\parallel\parallel} := t^a t^b A_{ab}$, for any symmetric tensor, A_{ab}. For the CH energy (9), with stress given by Eq. (53), we identify the forces transmitted along the three directions as

$$f_{\perp\perp} = \kappa/2 \left(K_{\perp\perp}^2 - (K_{\parallel\parallel} - C_0)^2\right) - \sigma \,, \tag{56a}$$

$$f_{\perp\parallel} = \kappa \ (K - C_0) \ K_{\perp\parallel} \,, \tag{56b}$$

$$f_{\perp} = -\kappa \nabla_{\perp} K \,, \quad \text{where} \quad \nabla_{\perp} = l^a \nabla_a \,. \tag{56c}$$

Note that $f_{\parallel\parallel}$ is given by $f_{\perp\perp}$ with $\parallel$ and $\perp$ interchanged; if the tangential bending stress is tensile along one direction (not necessarily a principal direction), it will be compressive along the orthogonal direction. There will generally be a geometrical in-plane shear $f_{\perp\parallel}$ if $K_{\perp\parallel} \neq 0$. There is, of course, no inconsistency with the fluid character of the membrane.

Whereas a fluid sphere may be stress free, a cylinder will generally be under tension along the axial direction (the curvature along the axis $K_{\perp\perp} = 0$ in Eq. (56a)). A cylinder thus needs to be supported by an external axial force to prevent its collapse along the axis. By scale invariance, this will necessarily be accompanied by contraction along the radial direction.

Like surface tension, spontaneous curvature breaks the scale invariance of the energy. Its presence introduces an additional contribution to the tangential stress, $f_S^{ab} = -\frac{1}{2}\kappa C_0^2 \, g^{ab} - \kappa C_0 \left(K^{ab} - K g^{ab}\right)$, but no normal stress. On a flat membrane, only the first term remains, so spontaneous curvature contributes isotropically to the tension, Lipowsky (2013); if the membrane is not flat, however, it makes an additional curvature dependent and generally non-isotropic contribution to the principal tangential stresses.

As Eq. (56) indicates, spontaneous curvature biases only the contribution of the transverse curvature to the forces transmitted across curves. A positive spontaneous curvature will thus reduce the axial tension required to support a cylinder. An appropriate spontaneous curvature will even allow tethers to form in the absence of external forces, Lipowsky (2013); Deserno (2015).

An alternative natural appearance of a term linear in K is in the bilayer couple model, which accommodates a fixed area difference between the two layers within the bilayer, Svetina and Žekž (1989); Svetina and Žekš (2014). Indeed, if the bilayer has a constant thickness t, the difference in area between its two sides is given by Eq. (22) to be $t \int dA \, K$. This model has been repurposed recently in the context of tetralayers consisting of pairs of parallel bilayers with different areas. As such, it could play a role in explaining the morphology of the rough endoplasmic reticulum or the nuclear envelope, Guven et al. (2014).

Historical note: the concept of a stress tensor for fluid membranes was first explored, in the small gradient approximation, some time ago by physicists, Evans and Skalak (1980); it was also examined by applied mathematicians and engineers, Jenkins (1977); Steigmann (1999) from a continuum mechanical point of view. It would be fair to say, however that its origins in geometry were overlooked. The conservation laws implied by Euclidean invariance appears to have been first understood by Kusner in the context of minimal and constant mean curvature surfaces,

Kusner (1991). Inexplicably, as recounted in Bernard (2015), pure mathematicians working on the Willmore functional (our symmetric bending energy), Willmore (1982) (proven in 2014, Marques and Neves (2014a, b)) were late to appreciate the implications of Euclidean invariance in this context.

Shape equation from the conservation law: We have discussed stress but we have yet to unpack the contents of the conservation law for $\mathbf{f}^a$. Naively, there appears to be a discrepancy: for whereas there is a single shape equation, we possess three conservation laws (indeed there are more to come). We first show that the shape equation is implied by the conservation of the stress tensor. Using the notation introduced in Eq. (50), we note that the projection onto the normal vector of the conservation law Eq. (49) gives

$$\mathcal{E} := \mathbf{n} \cdot \nabla_a \mathbf{f}^a = \nabla_a f^{\ a} - K_{ab} f^{ab} = 0\,. \tag{57}$$

Using the expression (53), this reproduces the shape equation for a fluid membrane, (39). The divergence is no longer evident. Even if we were to stop here, we now possess a better understanding of the shape equation: in equilibrium, the coupling of the tangential stress to curvature is the source of the normal stress.

External forces or normal constraints on the geometry will introduce sources on the right hand side of the conservation law. For instance, the source associated with an osmotic pressure is normal, given by $P\,\mathbf{n}$, so Eq. (39) is replaced by $\mathcal{E} = P$.

The projections of Eq. (49) along tangent directions implies

$$\mathcal{E}_b := \mathbf{e}_b \cdot \nabla_a \mathbf{f}^a = \nabla_a f^a_{\ b} + K_{ab} f^a = 0\,. \tag{58}$$

This is another constraint between the tangential and normal stresses: and it appear to suggest a symmetry between Eqs. (58) and (57) with tangential and normal stresses interchanged. The character of Eq. (58), however, is very different. In general, if the only degrees of freedom are geometric, this equation amounts always to a geometric identity; it hold for each term in the energy independently of the shape equation. To understand why this is so, recall that infinitesimal tangential deformations are identified with reparametrizations; using the fact that reparametrization acts by Lie derivation along the tangent vector field, this identity is reproduced for any geometrical invariant of the form (16) whether or not the geometry is equilibrated, Guven and Vázquez-Montejo (2013a).

More explicitly, using Eqs. (20a), we can write

$$\begin{aligned}\delta_\parallel H &= \int dA \left(-\frac{1}{2} T^{ab}\, \delta_\parallel g_{ab} + H^{ab} \delta_\parallel K_{ab}\right) \\ &= \int dA \, \left(\nabla_a f^{ab} + K^{ab} f_a\right) \Phi_b + \int dA \, \nabla_a (\mathcal{H} \Phi^a)\,,\end{aligned} \tag{59}$$

where we have used the definitions of the tangential and normal stresses given by Eq. (51). These are analogues of the contracted Bianchi identities in general relativity which follow from the general covariance of the Hilbert Einstein action.

Matters are less straightforward if local constraints are imposed on the geometry or material degrees of freedom interact with it. It also bears remarking that if the manifest reparametrization invariance is broken, choosing a parametrization adapted to the geometry such as the harmonic parametrization used in the Weierstrass–Enneper representation of a surface, which constrains the metric, Guven and Vázquez-Montejo (2010), the counterparts of Eq. (58) are no longer trivially satisfied. Instead they determine the additional Lagrange multipliers associated with this choice of gauge. It is only modulo this input that the counterpart of Eq. (57) reproduces the shape equation.

Isometric bending: A surprising application of the framework presented in Sect. 5 has been to the description of thin unstretchable sheets (think paper if $\mathcal{K}_G = 0$), an idealization that may be relevant in cell biology when proteins condense on a membrane. Whereas static fluid membranes shear freely; shear is impossible without stretching. The two limits, nonetheless, are described by the geometrical degrees of freedom of the surface. Unstretchability translates geometrically into the constraint that the metric be isometric to some fixed metric. This local congruence is accommodated in the variational principle by introducing a tensor-valued Lagrange multiplier $\mathcal{T}^{ab}$, and replacing H_C in Eq. (46) by[19]

$$H_C - \frac{1}{2}\int dA\, \mathcal{T}^{ab}(u^1, u^2)(g_{ab} - g^{(0)}_{ab})\,, \tag{60}$$

where $g^{(0)}_{ab}$ is this fixed metric. As a consequence, the tangential stress f^{ab} is replaced by $f^{ab} + \mathcal{T}^{ab}$, whereas the normal stress is unchanged. The significant point is that, even though no extra fields are introduced, the stress is no longer completely determined by the local geometry even though the degrees of freedom remain geometrical. The EL equation (57) is replaced by $\mathcal{E} - K_{ab}\mathcal{T}^{ab} = 0$. The presence of the isometry constraint also breaks the identification of tangential deformations with reparametrizations: The tangential projection of the conservation law (58) implies that the multiplier field $\mathcal{T}^{ab}$ is conserved: $\nabla_a \mathcal{T}^{ab} = 0$, Guven and Müller (2008); Guven et al. (2012).

In this context, it is worth looking at the weaker constraint, local incompressibility. The constraint (60) is replaced by

$$H_C - \frac{1}{2}\int d^2u\, \mathcal{A}(u^1, u^2)(\sqrt{g} - \sqrt{g^{(0)}})\,, \tag{61}$$

Now instead of $f^{ab} + \mathcal{T}^{ab}$, we have $f^{ab} + \mathcal{A}g^{ab}$, with an inhomogeneous stress. However, in equilibrium, the tangential conservation law (58) implies that $\mathcal{A}$ is constant; which is the same stress as that associated with a globally constrained area.

Tangential EL with material fields: Let there be material fields: this could be a scalar $S(u^1, u^2)$ or a vector field $V^a(u^1, u^2)$, so that the total energy density is replaced by $\mathcal{H}[g_{ab}, K_{ab}, V^a, S]$. The EL equations for these fields can be determined

[19] The local parametrization is fixed.

conventionally: $\mathcal{V}_a = 0$, $\mathcal{S} = 0$, where $\mathcal{V}_a = \delta H/(\delta V^a \sqrt{g})$ and $\mathcal{S} = \delta H/(\delta S\sqrt{g})$. Neither V^a nor S depends on $\mathbf{X}$, so that the identification of tangential deformations with reparametrizations breaks down for this $\mathcal{H}$. Now Eq. (58) is not reproduced by the argument leading to Eq. (59).

Suppose that V^a and S interact only with the intrinsic geometry and that $\mathcal{H}$ decomposes as $\mathcal{H} = \mathcal{H}(g_{ab}, K_{ab}) + \mathcal{H}_{\rm int}(g_{ab}, V^a, S)$, with correspond metric stress, $T^{ab} + T^{ab}_{\rm int}$. Now Eq. (58) implies $\nabla_a T^{ab}_{\rm int} = 0$, a nontrivial conclusion, Capovilla and Guven (2004a, b). The total stress associated with the fields on the Riemannian manifold described by the metric tensor g_{ab} is conserved. The surface itself does not even need to be in equilibrium.

Note that the conservation law does not necessarily imply the corresponding EL equations for the individual fields. If, however, the two fields do not couple directly, their tangential stresses decouple and are separately conserved. For example, suppose for simplicity that the scalar field is minimally coupled, described by the gradient energy plus a potential:

$$\mathcal{H}_I(g_{ab}, S) = \frac{1}{2} c\, g^{ab} \nabla_a S \nabla_b S + V(S)\,. \tag{62}$$

Now

$$T^{ab}_{\rm int}[g_{ab}, S] = c\left(\nabla^a S \nabla^b S - \frac{1}{2} g^{ab} g^{cd} \nabla_c S \nabla_d S\right) - g^{ab} V(S) \tag{63}$$

is conserved. This implies the EL equation for S,

$$-c\nabla^2 S + \partial V/\partial S = 0\,. \tag{64}$$

This equation involves the surface geometry only through its metric. The corresponding EL equation for the surface is modified by the addition of a source: $\mathcal{E} = 0$ in (57) is replaced by $\mathcal{E} - T^{ab}_{\rm int} K_{ab} = 0$. If instead of one scalar field we had two noninteracting fields, say S_1 and S_2, they will be separately conserved and their EL equations of the form (64) are uncoupled. Nonetheless the surface geometry mediates an interaction between these two fields through the shape equation: $\mathcal{E} - T^{ab}_{\rm int}[g_{ab}, S_1, S_2] K_{ab}$, where $T^{ab}_{\rm int}[g_{ab}, S_1, S_2] = T^{ab}_{\rm int}[g_{ab}, S_1] + T^{ab}_{\rm int}[g_{ab}, S_2]$. In particular in a three-component membrane (described by two relative concentration fields), one can anticipate nontrivial behavior associated with this indirect interaction. There is clearly a lot of nice physics yet to be unearthed, nevermind explored on this topic. A simple non-minimal coupling to curvature, such as a term of the form, $f(S)K$, will introduce a source in the EL equation for S.

Laplace pressure as effective surface stress: If there is a pressure difference P across the membrane, or the volume is fixed, there is an additional term in H given (modulo a possible constant) by $-PV$. Using Stokes theorem for the volume integral of the spatial identity, $\mathbf{div} \cdot \mathbf{x} = 3$, the volume can be expressed as a surface integral,[20]

[20] On a surface with boundary, this identity yields the volume of the cone standing on the surface patch, with its apex located at the origin.

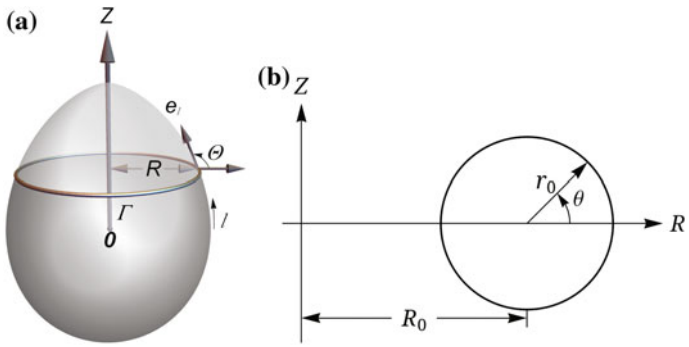

Fig. 3 **a** Parametrization of an axially symmetric surface. **b** Generating curve for a torus

$V = \frac{1}{3}\int dA\, \mathbf{X}\cdot\mathbf{n}$. However, the translational invariance of V implies that $\int dA\, \mathbf{n} = 0$, which in turn implies that $\mathbf{n}$ itself is a surface divergence. It is simple to verify that

$$\mathbf{n} = \nabla_a \mathbf{f}_L^a\,, \quad \text{where} \quad \mathbf{f}_L^a = \frac{1}{2}\mathbf{X}\times\left(\mathbf{n}\times\mathbf{e}^a\right)\,. \tag{65}$$

It follows that the Laplace force across the surface can, itself, always be treated as an effective surface stress tensor $-P\,\mathbf{f}_L^a$, Guven (2006).

Axially symmetric vesicles: In general, the EL equation cannot be integrated. Axial symmetry, however, implies the existence of a first integral of the shape equation which facilitates the identification of equilibrium states. The traditional way to identify this first integral is to adapt the variational principle to this symmetry, Zheng and Liu (1993); Jülicher and Seifert (1994); Podgornik et al. (1995). However, the conservation law provides an instructive alternative derivation in terms of the stresses shaping an axially symmetric geometry.

First, let us review a few essential properties of axially symmetric surfaces. The parallels and meridians on the surface form the principle directions. The curvatures along these directions are given respectively by $C_\parallel = \sin\Theta/R$ and $C_\perp = \dot{\Theta}$, where R is the polar radius, Θ is the angle that the tangent along the meridian makes with the polar direction, and a dot represents a derivative with respect to arc length along the meridian, $\dot{} = d/dl = \nabla_\perp$, as indicated in Fig. 3a. Substituting into Eq. (56), we identify the nonvanishing tangential and normal forces per unit length transmitted across a parallel from the membrane below it, $f_{\perp\perp}$ and $f_\perp$ respectively.

We now use the conservation law to identify the first integral: first project $\nabla_a \mathbf{f}^a = P\mathbf{n}$ onto the symmetry axis; now integrate over the source-free region bounded below by a given parallel circle. Using Stokes theorem on the left-hand side, we find that the linear combination of stresses

$$\mathcal{L} := \sin\Theta f_{\perp\perp} - \cos\Theta f_\perp\,, \tag{66}$$

satisfies

$$\mathcal{L} = PR/2 + C/(2\pi R)\,, \tag{67}$$

on this circle, where C is a constant of integration. Note how the derivative is peeled off $f_\perp$ in this construction. This equation, first written down in Capovilla and Guven (2002b) (but without the important constant C), expresses equilibrium in terms of an algebraic balance of tangential and normal stresses. The constant is identified as the total external axial force acting from above; an equal and opposite force must counteract it somewhere else. In the absence of such a force, $C = 0$. We will examine one situation where it vanishes (even though radial external forces act on the vesicle) and two where it does not: one for topological reasons; the other due to external axial forces bearing down on the poles of a vesicle.

Stress and Torque conservation from Euclidean invariance: It is straightforward using the auxiliary framework to show that the change in energy under a deformation of the surface $\delta\mathbf{X}$ is given by

$$\delta H[\mathbf{X}] = \int dA\, \mathcal{E}\, \mathbf{n}\cdot\delta\mathbf{X} + \int dA\, \nabla_a \left[-\mathbf{f}^a\cdot\delta\mathbf{X} + H^{ab}\mathbf{e}_b\cdot\delta\mathbf{n}\right]. \tag{68}$$

This identity follows from the first variation of Eq. (46): the first term on the right in Eq. (68) involves the EL derivative with respect to $\mathbf{X}$ and it vanishes in equilibrium if the region is source-free; the second term collects in a divergence the two terms linear in derivatives, $\partial_a\delta\mathbf{X}$ and $\partial_a\delta\mathbf{n}$, appearing in δH_C when $\mathbf{X}$ and $\mathbf{n}$ are varied. On any patch of free surface, it depends only on the boundary behavior of the stress, $\mathbf{f}^a$, and the response to changes in the curvature, H^{ab}; this is not an accident.

Using Eq. (68), it is simple to reproduce the conservation law for the stress tensor, Eq. (49). For under a constant translation $\delta\boldsymbol{a}$, the energy is unchanged within any surface patch so that $\delta H = 0$; as a result, $\delta\boldsymbol{a}\cdot\int dA\,\nabla_a\mathbf{f}^a = 0$. Because the patch is arbitrary, the integrand must vanish pointwise, reproducing the conservation law. This is not surprising: translational invariance was already manifest in the variational principle.

The rotational invariance, on the other hand, was not. Under a constant rotation $\delta\boldsymbol{\omega}$, one has $\delta\mathbf{X} = \delta\boldsymbol{\omega}\times\mathbf{X}$ and $\delta\mathbf{n} = \delta\boldsymbol{\omega}\times\mathbf{n}$ so that, in equilibrium, $\delta\boldsymbol{\omega}\cdot\int dA\,\nabla_a\mathbf{m}^a = 0$, where

$$\mathbf{m}^a = \mathbf{X}\times\mathbf{f}^a + H^{ab}\,\mathbf{e}_b\times\mathbf{n}\,. \tag{69}$$

Thus, $\mathbf{m}^a$, which is identified as the surface torque tensor, Capovilla and Guven (2002b); Müller et al. (2007), is also conserved: $\nabla_a\mathbf{m}^a = 0$. The first term appearing in $\mathbf{m}^a$ represents the moment of the local stress, whereas the second term—the bending moment—is position independent, a contribution originating in the curvature dependence of the energy.

Consider the effect of a scaling $\delta\mathbf{X} = \lambda\mathbf{X}$ on any functional of the form (16): now Eq. (68) implies

$$\delta H[\mathbf{X}] = \lambda \int dA\, \mathcal{E}\, \mathbf{n} \cdot \delta \mathbf{X} - \lambda \int ds\, \mathbf{f}_\perp \cdot \mathbf{X}\,. \tag{70}$$

Suppose that H has a consistent scaling dimension. If $H = A$, then $H[\Lambda \mathbf{X}] = \Lambda^2 H[\mathbf{X}]$. furthermore $\mathcal{E} = K$. and $\mathbf{f}^a = -g^{ab}\mathbf{e}_b$. One identifies

$$2A = \int dA\, K\, \mathbf{n} \cdot \mathbf{X} + \int ds\, \mathbf{l} \cdot \mathbf{X}\,. \tag{71}$$

This is the Jellett–Minkowski identity, identified by Jellett mid-nineteenth century but usually attributed only to the latter mathematician, Jellett (1853). A corollary is that there do not exist closed minimal surfaces.

Stresses in the Monge representation: It is instructive to compare the manifestly covariant framework described here with its counterpart using the height function representation of the surface, treating the energy as a functional of this scalar field on the reference plane. We now examine the forces and torques along this plane and orthogonal to it.

One can exploit the Euclidean invariance of the energy with respect to translations on the base plane, exactly as one does for a classical scalar field (electrostatics say), to identify the conserved horizontal stress. But we do not need to: because we can also project $\mathbf{f}^a$ onto the base plane. In the quadratic approximation, this stress is given by, Fournier (2007)

$$T_{ij} = \kappa T^B_{ij} + \Sigma T^0_{ij}\,, \tag{72}$$

where

$$T^B_{ij} \approx \nabla^2 h \left(\partial_i \partial_j h - \frac{1}{2}\nabla_0^2 h \delta_{ij}\right) - \partial_i(\nabla_0^2 h)\partial_j h\,, \tag{73}$$

and

$$T^0_{ij} \approx -\left(1 + (\nabla_0 h)^2/2\right)\delta_{ij} + \partial_i h\, \partial_j h\,. \tag{74}$$

Not surprisingly, modulo the constant term associated with the area of the base plane, T^0_{ij} assumes the form of the stress tensor of a free scalar field h on the plane. Compare Eq. (74) with (63). We observe also that T^B_{ij} is not symmetric so that, whereas $\partial_i T_{ij} = 0$, if the indices are switched the divergence does not vanish: $\partial_i T^B_{ji} \neq \partial_i T^B_{ij}$. There is no such ambiguity in the reparametrization invariant approach. Notice also that in T^0_{ij} neither homogeneity nor isotropy are manifest. This apparent spatial variation is an artifact of the planar projection.[21] Already in this simple setting, one can see the advantage of possessing the covariant description. Even if one decides to perform calculations in the height function representation, the covariant approach provides

[21] Intriguingly, the quadratic contribution to T^B_{ij} is trace-free in this approximation, a property we would associate with scale invariance. Yet the area itself is clearly not scale invariant. The source of this peculiarity is that, in the quadratic approximation in gradients of h, the area is represented by a massless two-dimensional scalar field on the plane which is scale invariant if the plane is scaled, but not if h is. On the other hand, T^B_{ji} is not trace-free but should not have been expected to be.

an unambiguous statement about the nature of the underlying stress. The apparent discrepancies using height functions arise because T_{ij} is not the physically significant tangential stress but its projection onto a plane and the fact that heights are treated differently from locations on this plane.

The conserved normal force density is $N_i = \kappa\partial_i(\nabla_0^2 h) - \sigma\partial_i h$. The conservation laws for T_{ij} and N_i together encode the information content of Eq. (49), correct to quadratic order. As we saw, they are not independent.

The invariance of the energy with respect to rotations about an axis orthogonal to the base plane implies the conservation of the vertical torque,

$$M_i = \kappa\left(\nabla^2 h - C_0\right)\varepsilon_{ij}\partial_j h + \bar{k}\left(\nabla^2 h\varepsilon_{ij} - \partial_i\partial_k h\varepsilon_{kj}\right)\partial_j h\,. \tag{75}$$

To account for the full rotational invariance of the surface energy, one needs to consider rotations about two orthogonal axes lying in the plane. This involves the rotation of the base plane itself, conflating the scalar field and the reference geometry, a symmetry without any analogue in the theory of a scalar field on the plane. This is probably why this was not considered in the height function until recently, Fournier (2007), several years after the covariant description. Taking the appropriate projections, we identify the horizontal torques

$$M_{ij} = \kappa\left(\nabla^2 h - C_0\right)\varepsilon_{ij} + \bar{\kappa}\left(\varepsilon_{ij}\,\nabla^2 h - \varepsilon_{ik}\partial_k\partial_j h\right)\,. \tag{76}$$

Forces and torques without gauges: In biology, membranes are invariably shaped by external forces or constraints; often these act locally: for example, the final stage of endocytosis may involve the constriction of membrane necks by dynamin spirals, Kozlov (2001); Morlot and Roux (2013); McDargh et al. (2016). There has also been a considerable amount of work on the interactions between membrane bound particles (read proteins) that are mediated by the deformed membrane geometry, Goulian et al. (1993); Kralj-Iglič et al. (1996, 1999); Weikl et al. (1998); Kim et al. (1998); Yolcu et al. (2011, 2012); Yolcu and Deserno (2012); Fournier (2014); Haussman and Deserno (2014); Božič et al. (2015); Fournier and Galatola (2015); Schweitzer and Kozlov (2015). The covariant stress tensor has also been shown to provide insight into these processes, permitting one to understand non-perturbative behavior, without the need to resort to triangulations or simulations, Müller et al. (2005a, b); it also provides a rigorous framework guiding the design of the computational setup and the interpretation of results, Reynwar et al. (2007). The subject of membrane fluctuations or Casimir forces has received considerable attention and has been the subject of reviews, Deserno (2009); Yolcu et al. (2014). It would also appear that the covariant language is the natural one to use in order to progress beyond the quadratic or Gaussian approximation in height functions in this context. The geometrical nature of the problem indicates that these corrections will involve geometrical invariants.

In this section, we show how the forces and torques acting on the membrane (or transmitted by it) are identified in our framework. Consider a number of localized sources acting on the membrane. These could also be particles interacting with the

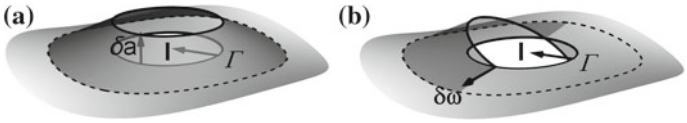

Fig. 4 Local **a** translation and **b** rotation of the contours enclosing localized sources on the membrane. The vector **l** is the normal to the contour Γ pointing into the source. Their magnitude has been exaggerated for illustration purposes

membrane. To identify the force on the membrane associated with any particular source, one needs to determine the change in the energy when this source alone is displaced. This sounds like a complicated operation because its displacement will drag the membrane along with it. Fortunately, we are only interested in deformations around equilibrium, so to first order the membrane deformation turns out to be irrelevant. We thus let $\delta\mathbf{X}$ be *any* deformation reducing to a constant vector $\delta\mathbf{a}$ on the curve Γ bounding one of these sources while vanishing on all other boundaries, as illustrated in Fig. 4a. Now we use Stokes theorem in Eq. (68) to recast the divergence as an integral along Γ. The change in the energy of the membrane is then given by the intuitively simple expression:

$$\delta H = -\delta\mathbf{a}\cdot\mathbf{F}\,;\quad \mathbf{F} = \int_\Gamma ds\ \mathbf{f}_\perp\,. \tag{77}$$

where $\mathbf{f}_\perp$ was defined below Eq. (49). This is the work done on the membrane by the source inside Γ when it is displaced a distance $\delta\mathbf{a}$; as such, the vector $\mathbf{F}$ is identified as the force on the source (or particle), or equivalently minus the force on the membrane, Müller et al. (2005a, b); importantly, it is determined completely by the surface geometry in the neighborhood of this boundary. What exactly is occurring inside Γ is irrelevant, it may be treated as a black box. If there is membrane inside, and we decide to look inside, the distribution of the normal force acting on it is given by $\mathcal{E}\,\mathbf{n}$, and the total force (not necessarily normal) is determined by integrating over the interior of Γ covered by membrane, Phillips et al. (2009). Of course, any geometry subjected to appropriate sources represents an equilibrium: simply evaluate $\mathcal{E}$ to determine them. There is, however, no guarantee that such sources will be physical.

Note that the integrated conservation law over the free surface implies Newton's third law: if there are N boundaries with associated forces $\mathbf{F}_I$, $I = 1, \ldots, N$, then

$$0 = \int dA\ \nabla_a \mathbf{f}^a = \sum_{I=1}^{N} \mathbf{F}_I\,. \tag{78}$$

The torque associated with an external source can be identified by examining the response of the energy to a rigid rotation of the source. Under a rigid infinitesimal rotation of Γ through an angle $\delta\boldsymbol{\omega}$, the corresponding change in the energy is

$$\delta H = -\delta\boldsymbol{\omega}\cdot\mathbf{M}\,,\quad \mathbf{M} = \int_\Gamma ds\,\mathbf{m}_\perp\,, \tag{79}$$

where $\mathbf{m}_\perp = l_a\mathbf{m}^a$ and $\mathbf{m}^a$ was defined in Eq. (69). The Gaussian term in the CH energy contributes through H_G^{ab} to $\mathbf{m}^a$, Fournier (2007). It also plays an important role in the local boundary conditions. However, it does not contribute to the total torque: this is because the corresponding contribution to $\mathbf{m}_\perp$ is proportional to the arc length derivative of the surface normal vector along the boundary, $\mathbf{m}_\perp = \bar{\kappa}\mathbf{n}'$, and thus integrates to zero.

In a manner analogous to that for $\mathbf{f}_\perp$, with an obvious notation, we can express $\mathbf{m}_\perp = m_{\perp\parallel}\mathbf{T} + m_{\perp\perp}\mathbf{l} + m_\perp\mathbf{n}$. Along a parallel circle on an axially symmetric geometry, the only surviving component is $m_{\perp\parallel}$, given by

$$m_{\perp\parallel} = f_{\perp\perp}\mathbf{X}\cdot\mathbf{n} - f_\perp\mathbf{X}\cdot\mathbf{l} - H_{\perp\perp}\,. \tag{80}$$

The conservation laws for stress and torque imply that the integrals in (77) and (79) will be identical on any contour homotopically equivalent to Γ outside of sources. In particular, if the geometry possesses symmetries, the contour can also be deformed to exploit these symmetries. This stratagem was used to determine the forces and torques mediated by the membrane between identical particles on a membrane, Müller et al. (2005a, b). One has, perhaps unsurprisingly, nonlinear analogues of Gauss' law in electrostatics.

Horizontal force on the ramp dipole: The line integral (77) permits one to determine the horizontal force between two elements of the minimal dipole discussed earlier. One can show that it is always attractive, and given in the small gradient approximation by (T^0_{ij} is defined in Eq. (74))

$$F = \sigma\int dy\,T^0_{xx} = \frac{1}{2}\Sigma\int dy\,(\partial_y h)^2 = 2\pi p^2\Sigma/R\,. \tag{81}$$

Geometrically, this is the length added to the midline, Guven et al. (2014). Minimal ramps of opposite chiralities attract; if they were the same, they would repel, Müller et al. (2005a). To prove this note that the contour can be deformed so as to coincide with the "square" Γ illustrated in Fig. 1a. As shown in Guven et al. (2014), the minimal dipole is stabilized by nonharmonic corrections. The simplest example involves the local addition to each helicoid of the solution to the Helmholtz equation, $h \approx K_0(\lambda r)\,\varphi$, described earlier. The integrated stress associated with such a correction is always negative which implies repulsion. The dipole size is set by the competition between this short range repulsion (associated with bending) and the long range attraction associated with tension.

Note that the behavior of the minimal ramp persists in the nonlinear theory, Müller et al. (2005a). For a minimal dipole, the force on either ramp is given by $\mathbf{F} = \Sigma\int_\Gamma ds\,\mathbf{l}$. By symmetry, the force is given by $\Sigma\Delta L$, where ΔL is—as before—the length added to the midline.

It bears emphasizing that, even in the linearized theory, this approach always outperforms the approach still overwhelmingly used in this field to determine forces which requires integrating the energy density over the entire surface and then differentiating with respect to the placement of the sources. Here, it is sufficient to know the geometry in the neighborhood of a single bounding curve: avoiding the unnecessary integration and subsequent differentiation.

Boundary conditions: If the free surface terminates on a free boundary, with an associated line tension or its own bending energy, the second term in Eq. (68) provides the appropriate boundary conditions, circumventing the necessity to reevaluate them anew every time we have a boundary to contend with. The explicit use of the stress tensor in this context was first made in Capovilla et al. (2002). An elegant derivation of these boundary conditions, including not only boundary tension but also boundary bending energy, using the methods of exterior differential calculus was provided in Tu and Ou-Yang (2003, 2004).

If an interface separates two phases with distinct physical parameters, the difference in the contributions from the two permits one to identify the appropriate matching conditions, Müller (2007). If the membrane adheres to a substrate, with a contact potential, (68) facilitates the identification of the discontinuity in the normal curvature at the boundary of the region of contact, Capovilla and Guven (2002a). A rather more comprehensive treatment of the adhesion process using the framework presented here is given in Deserno et al. (2007).

Surfaces as emergent: An alternative to the auxiliary route to the shape equation is again to focus on g_{ab} and K_{ab} as independent tensor fields but, instead of the structure equations, to impose the Gauss–Codazzi and Codazzi–Mainardi equations as constraints, Guven and Vázquez-Montejo (2013a). This approach, as we will see, has some surprising consequences.

Consider a Riemannian manifold with a metric g_{ab} (there is a whiff of gravity here), coupling to a symmetric tensor K_{ab}. If these two tensor fields satisfy the Gauss–Codazzi and Codazzi–Mainardi equations (29), they describe the induced metric and extrinsic curvature on a surface embedded in three-dimensional Euclidean space, Spivak (1999). We thus see that these equations are both necessary and sufficient conditions for forming a surface.

It is now possible, in principle, to address geometric questions about surfaces without any explicit reference to its environment; the surface itself is an emergent equilibrium entity. In this approach one does not have a surface to speak of away from equilibrium.

In contrast with the auxiliary approach, there is even no need to introduce the embedding, $\mathbf{X}$, explicitly in the variational principle. Let us replace $H[\mathbf{X}] = \int dA\, \mathcal{H}[g_{ab}, K_{ab}]$ by

$$H_c[g_{ab}, K_{ab}, \Lambda, \lambda^a] = H[g_{ab}, K_{ab}] + I[g_{ab}, K_{ab}, \Lambda, \lambda^a]\,, \tag{82}$$

where

$$I = \frac{1}{4}\int dA\, \Lambda\, \mathcal{C}_\perp - \frac{1}{2}\int dA\, \lambda^a \mathcal{C}_a\,, \tag{83}$$

with $\mathcal{C}_\perp := \mathcal{R} - K^2 + K_{ab}K^{ab}$ and $\mathcal{C}^a := \nabla_b(K^{ab} - g^{ab}K)$. The multiplier fields Λ and λ^a enforce Eq. (29) permitting g_{ab} and K_{ab} to be treated as independent variables. Notice that K_{ab} will tag along even if H depends only on g_{ab}, such as it does in an interfacial energy. For the reader familiar with general relativity, I has all the appearance of the Arnowitt–Deser–Misner (ADM) action in the Hamiltonian formulation of the theory, Arnowitt et al. (1959). This is a two-dimensional accident! For if we were genuinely working in four dimensions, we would need to replace the single Gauss–Codazzi equation by the twenty equations (33), and Λ by a tensor-valued Λ^{abcd}, with the symmetries of the Riemann tensor. Curiously, the Codazzi–Mainardi equations in four and higher dimensions are completely determined by their Gauss–Codazzi counterparts (Thomas) so that the corresponding multipliers are redundant: $\lambda^a \to \lambda^{abc} = 0$.

Remarkably, one never needs to identify these multiplier fields explicitly in the derivation of the shape equation.

Instead of $\mathbf{X} \to \mathbf{X} + \delta\mathbf{X}$, we have

$$\delta(H + I) = \int dA \left[-\frac{1}{2}(T^{ab} + \mathcal{T}^{ab})\,\delta g_{ab} + (H^{ab} + \mathcal{H}^{ab})\,\delta K_{ab} \right] + BT \tag{84}$$

where T^{ab} and H^{ab} are the functional derivatives of H wrt g_{ab} and K_{ab} defined earlier; $\mathcal{T}^{ab}$ and $\mathcal{H}^{ab}$ are the counterparts for the constraint term I. BT represents terms collected in a divergence after integration by parts. The equilibrium states of the surface are described by the coupled pdes on the two-dimensional Riemannian manifold:

$$T^{ab} + \mathcal{T}^{ab} = 0\,; \tag{85a}$$
$$H^{ab} + \mathcal{H}^{ab} = 0\,, \tag{85b}$$

supplemented with $\mathcal{C}_\perp = 0$ and $\mathcal{C}_a = 0$. Equation (85a) are the analogues of the Einstein equations. Equation (85b) are their counterparts for K_{ab}.

The EL derivatives, $\mathcal{T}^{ab}$ and $\mathcal{H}^{ab}$, originating in the constraints are model independent. Both are linear in $\mathcal{L}_{\mathbf{\Lambda}} g_{ab}$ and $\mathcal{L}_{\mathbf{\Lambda}} K_{ab}$:

$$\begin{aligned} \mathcal{T}^{ab} &= \frac{1}{4}\left(g^{ab}K^{cd} - g^{cd}K^{ab}\right)\,\mathcal{L}_{\mathbf{\Lambda}} g_{cd} \\ &\quad + \frac{1}{2}\,\left(g^{ac}g^{bd} - g^{ab}g^{cd}\right)\,\mathcal{L}_{\mathbf{\Lambda}} K_{cd}\,; \end{aligned} \tag{86a}$$
$$\mathcal{H}^{ab} = \frac{1}{4}\left(g^{ac}g^{bd} - g^{ab}g^{cd}\right)\mathcal{L}_{\mathbf{\Lambda}} g_{cd}\,, \tag{86b}$$

where

$$\mathcal{L}_{\mathbf{\Lambda}} g_{ab} = 2K_{ab}\Lambda + \mathcal{L}_\lambda g_{ab}\,; \tag{87a}$$
$$\mathcal{L}_{\mathbf{\Lambda}} K_{ab} = \left(-\nabla_a\nabla_b + K_{ac}K^c{}_b\right)\Lambda + \mathcal{L}_\lambda K_{ab}\,. \tag{87b}$$

If we consult Eqs. (19) and (20a), and restore our Euclidean background, then $\mathbf{\Lambda} = \Lambda\,\mathbf{n} + \lambda^a\,\mathbf{e}_a$ is identified as the generator of a surface displacement with the identification of Λ with Φ and λ^a with Φ^a in (18). But remember that here λ^a and Λ are the generalized forces coupling the two fields to form a surface. Their role is not to displace.

To identify the shape equation, the contraction of Eq. (86) provides a very useful identity:

$$K_{ab}\mathcal{T}^{ab} = \frac{1}{4}\left(g^{ab}\nabla^2 - \nabla^a\nabla^b + K^{ac}K_c{}^b - g^{ab}K_{cd}K^{cd}\right)\mathcal{L}_{\mathbf{\Lambda}}g_{ab}\,, \tag{88}$$

equating the contraction $K_{ab}\mathcal{T}^{ab}$ to a differential expression linear in $\mathcal{L}_{\mathbf{\Lambda}}g_{ab}$. Significantly, $\mathcal{L}_{\mathbf{\Lambda}}K_{ab}$ does not appear.

Now let us apply this framework to *gravitational impostors*, described by a Hamiltonian depending only on the metric, $H = H[g_{ab}]$. Now $H^{ab} = \delta H/\delta K_{ab} = 0$ so that Eq. (85b) implies that $\mathcal{H}^{ab} = 0$ as well. But the identity (86b) then implies that $\mathcal{L}_{\mathbf{\Lambda}}g_{cd} = 0$ or that $\mathbf{\Lambda}$ generates surface isometries. The identity (88) now implies that $K_{ab}\mathcal{T}^{ab} = 0$. The Einstein equations Eq. (85a) finally imply that $-K_{ab}\,T^{ab} = 0$: an unusually short story.

For the trivial example of an interface, $H = \sigma A$, with $T^{ab} = -\sigma g^{ab}$, we reproduce the equation, $K = 0$. The stationary states are minimal surfaces.

This is somewhat mysterious. The Lagrange multipliers appear to have been very obliging: in the derivation of the surface EL equations, they do their job but we never even need to identify $\mathbf{\Lambda}$ explicitly. But let's look at them. For the area, $H = \sigma A$, the trace of T^{ab}, $T^a{}_a = -2\sigma$. Equation (86) implies that $\mathcal{T}^a_a = -\frac{1}{2}\,\mathcal{L}_{\mathbf{\Lambda}}K$. But $\mathcal{L}_{\mathbf{\Lambda}}K = \left(-\nabla^2 + \mathcal{R}\right)\Lambda$, so that

$$\left(-\nabla^2 + \mathcal{R}\right)\Lambda = -4\sigma \tag{89}$$

The determination of Λ decouples from that of λ^a. One can show that the appropriate boundary conditions are $\Lambda = 0$. Because Eq. (89) is inhomogeneous, the isometry will be nontrivial! It is also uniquely determined by the equilibrium geometry.

The differential operator $\mathcal{D} = -\nabla^2 + \mathcal{R}$ also appears in the second variation of the area:

$$\delta^2 A = \int dA\,\Phi\,\mathcal{D}\,\Phi\,, \tag{90}$$

where Φ is the normal deformation of surface. To see this use Eq. (36) to obtain for the second variation of the area about an equilibrium, $\delta^2 A = \int dA\,\Phi\,\delta_\perp K$. Using Eq. (37) for $\delta_\perp K$ we recover Eq. (90). Negative eigenvalues signal instability.

Now let us look at solutions of Eq. (89). In particular, consider a catenoid of neck radius R_0, parametrized $R(l)/R_0 = \sqrt{1 + (l/R_0)^2}$, $Z(l) = \operatorname{arcsinh} l/R_0$, bounded between 2 rings separated a distance $2L$ along the meridian. There exists an exact solution for Λ, negative everywhere, vanishing on the boundaries, with a minimum on the neck, as illustrated in Fig. 5b, Guven and Vázquez-Montejo (2013a). The solution diverges as $L \to 1.5088R_0$.

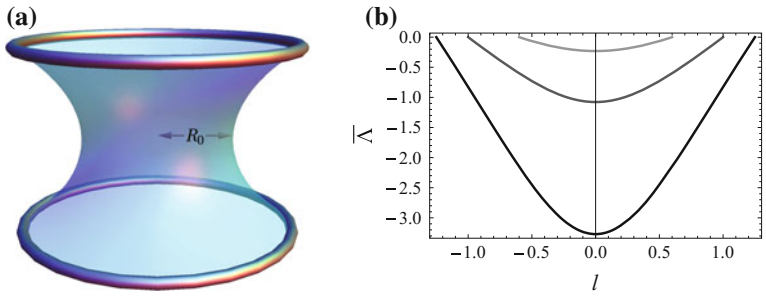

Fig. 5 **a** Soap Bridge **b** Λ versus l

Now look at the spectrum of the operator $\mathcal{D}$: $(-\nabla^2 + \mathcal{R})\Phi_n = E_n \Phi_n$, $E_0 < E_1 < E_2 < \cdots$. If L is small, $E_0 > 0$. The spectral expansion of Λ, $\Lambda = \sum \Lambda_n \Phi_n$, indicates that $\Lambda \to \infty$ correlates with $E_0 \to 0$. Singularities in Λ correlate with the onset of instability. A new criterion is identified for the onset of surface instability. This is an intuitive result: instabilities are reflected in our inability to find an equilibrium pair, g_{ab} and K_{ab}, satisfying Eq. (29).

6 External Forces and Nontrivial Topology

In this section we present examples of surface states minimizing the CH energy when the geometry is subjected to localized external forces or topological constraints, analyzing the connection between the stress and the geometry using the framework presented here. The first example considers the response of a spherical vesicle, of fixed area, to the radial constriction of its equator. We next present new insight into an old problem: the equilibrium of toroidal vesicles; we show how the topology provides sources for both forces and torques in the vesicle, and describe the distribution of stress associated with these sources. Finally, we demonstrate how the conformal invariance of the bending energy can be exploited to examine the morphologies of a vesicle (not necessarily axially symmetric) subjected to localized external forces bringing two points (or small patches) into contact.

6.1 Constriction of a Spherical Vesicle

If the membrane possesses spherical topology, and is free of axial forces, then $C = 0$ on the right side of Eq. (67). Let the vesicle have a fixed area $A_0 = 4\pi R_0^2$, and be subjected to an equatorial constriction provided by an external rigid ring of radius r_0. To keep matters simple, we do not admit spontaneous curvature or fix the volume. There are no axial forces, so $\mathcal{L} = 0$ (with $C_0 = 0$) in Eq. (67) everywhere except

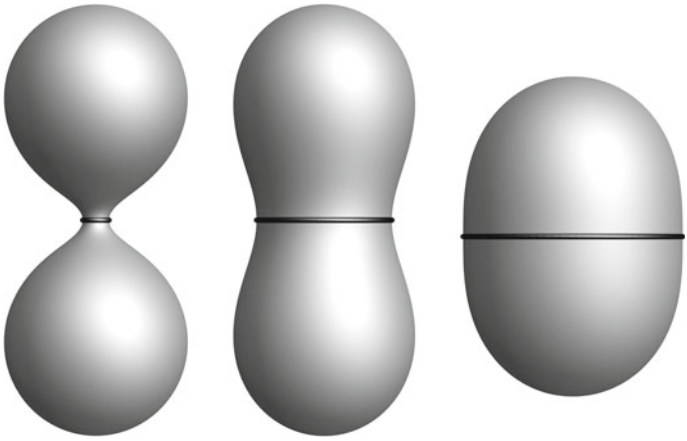

(a) $r_0 = 0.1\,R_0$ (b) $r_0 = 0.5\,R_0$ (c) $r_0 = 0.84\,R_0$

Fig. 6 Equatorial constriction of a spherical vesicle

along the equator where there is a radial source. The equation $\mathcal{L} = 0$ is solved by the shooting method for values of $0 \leq r_0 \leq R_0$. The one free parameter is σ, which is tuned to fix the area to A_0. As r_0 is decreased one observes the following morphological sequence: if the constriction is moderate ($0.84 \leq r_0/R_0 < 1$) the deformation is prolate, represented in Fig. 6c; if $0.2 \leq r_0/R_0 \leq 0.84$ the vesicle develops a waist as illustrated in Fig. 6b[22]; if r_0 is reduced further, so that $r_0/R_0 \leq 0.2$, the geometry morphs into two spherical lobes connected by an increasingly narrow neck (Fig. 6a); in the limit $r_0 \to 0$, it resembles two touching spheres of radius $R_0/\sqrt{2}$. Various questions suggest themselves. What is the geometry in the small neck connecting these two spheres and what is the force squeezing this neck? This force is nonvanishing, i.e., there are sources; thus the neck cannot be a catenoid. How then does it differ?

If the traction along the edge instead were outward, the vesicle would tend to become increasingly oblate as r_0 is increased, tending to a limiting geometry formed by two flat disks of radius $\sqrt{2}\,R_0$, glued together along their common perimeters with diverging energy and force. The force constricting the membrane is completely encoded in the membrane geometry in the neighborhood of the equator. To see this, consider the change in energy under a radial deformation of the equator, $\delta\mathbf{X} = \delta c\,\hat{\mathbf{r}}$. Using Eq. (68), one finds that $\delta H = -\delta c\,F$, where the equatorial constriction F is given by the jump across the equator at $l = 0$:

$$\frac{F}{2\pi r_0 \kappa} = \Big[-\sin\Theta\, f_\perp + \cos\Theta\, f_{\perp\perp} \Big]_{-\epsilon}^{\epsilon}. \tag{91}$$

[22] Unlike the prolate, this geometry is stable with respect to membrane slippage under the ring.

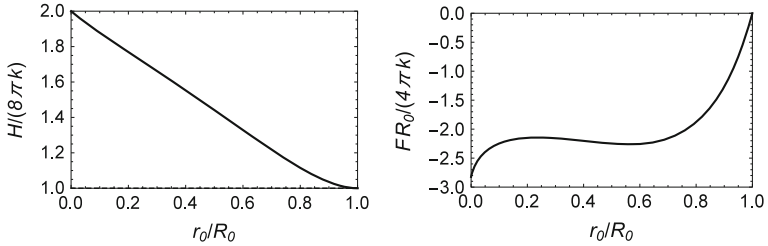

Fig. 7 Total energy and radial compression as functions of the ring radius. The bending energy increases monotonically as the equator is constricted, tending to the value $16\pi\kappa$ as $r_0 \to 0$; in contrast, the radial compression, does not behave monotonically

The tangent angle $\Theta = \pi/2$ so that the two contributions are equal and opposite:

$$\frac{F}{2\pi r_0 \kappa} = C'_{\perp 0}\Big|_{-\epsilon}^{\epsilon} = 2\Theta_0'' \,. \tag{92}$$

The presence of the force is signaled by a discontinuity in the derivative of the normal (meridian) curvature. along the equator. An alternative derivation is provided in Božič et al. (2014). Contrast this with line tension where the discontinuity is in the curvature $C_\perp$ itself.

Note that total equatorial force on the vesicle vanishes, in much the same way as the total Laplace force vanishes on a closed vesicle does, $\int dA\, \mathbf{n} = 0$. There is also an intriguing duality between the functional form of the expression within parenthesis in Eq. (91) and the first integral, $\mathcal{L}$ given by Eq. (66).

Notice that, whereas the energy increases almost linearly with r_0, the dependence of F on r_0 illustrated in Fig. 7b is non-monotonic; its behavior displays a striking correlation with the morphological changes in the membrane, increasing in magnitude as the membrane becomes prolate; relaxing slowly as the belt tightens but increasing again as the two lobes develop. In particular, not only is it nonvanishing in the limit $r_0 \to 0$, its magnitude is a global maximum. Using the equation, $\mathcal{L} = 0$, it is simple to show that the polar radius can be expanded $R(l)/r_0 \approx 1 + (\ell/r_0)^2 + F_0\, \pi r_0 |\ell/r_0|^3/12$ at the neck, when $r_0/R_0 \ll 1$, indicating explicitly the curvature derivative singularity (the third derivative) proportional to the limit force F_0. Significantly, it is not approximated by a catenoid of neck radius r_0, which is given exactly by $R(l)/r_0 = 1 + (\ell/r_0)^2$.

We have already seen that the scale invariance of the bending energy has physical implications. The constricted vesicle involves two scales, R_0 defined by the area, and the equatorial radius, r_0. The corresponding constraints can be introduced explicitly into the variational principal so that the unconstrained functional to be minimized is

$$H[\mathbf{X}] = H_{CH}[\mathbf{X}] + \sigma\,(A - 4\pi R_0^2) + \int ds\, \mathcal{F}(s)\,(|\mathbf{X}| - r_0)\,. \tag{93}$$

The function $\mathcal{F}(s)$ is a new local Lagrange multiplier enforcing the constraint on the equatorial radius. If axial symmetry is relaxed it will not be constant. If this constraint is removed, then $\sigma = 0$, a consequence of the scale invariance of bending energy. In equilibrium, one identifies $F := \int ds\, \mathcal{F}(s) = \partial H_B/\partial r_0$. This is the familiar expression involving H_B, and thus requiring knowledge of the complete vesicle geometry.

On casual inspection, Fig. 7a would suggest that H_B depends linearly on r_0. The wiggles may be small but they are real, as comparison with Fig. 7b indicates.

Consider now the effect of a membrane rescaling $\mathbf{X} \to \Lambda\mathbf{X}$ on H. One has

$$H[\Lambda\mathbf{X}] = H_{CH}[\mathbf{X}] + \sigma\,(\Lambda^2\,A - 4\pi R_0^2) + \int ds\,\mathcal{F}(s)\,\Lambda(\Lambda|\mathbf{X}| - r_0)\,. \tag{94}$$

In equilibrium $dH/d\Lambda = 0$ when $\Lambda = 1$. This implies that $r_0\,F = -2\sigma A$: σ thus also determines the force; its sign correlating with it. Note that σ vanishes in the limit $r_0 \to 0$. Elementary calculus then implies that the limiting traction is given by $F_0 = \lim_{r_0\to 0} \partial\sigma/\partial r_0$, reflecting the scale-free nontrivial neck geometry lurking in this limit.[23]

The model presented here is a very simplified description of the physics: the ring is assumed rigid. If the ring is elastic, it need not remain circular, and the contraction process will involve non-axially symmetric deformations of the vesicle. Modeling the constriction of a membrane neck by a dynamin spiral will necessarily involve both the breaking of axial symmetry as well as the deformation of the spiral, Nam et al. (2012); McDargh et al. (2016).

6.2 *Topology as a Source of Stress*

Nontrivial topology can also provide a source of stress. On a torus, closed curves along both the wheel and tube are homotopically nontrivial. Such geometries are not only of academic interest: toroidal vesicles were first observed experimentally some time ago, not only the common or garden single-holed variety, Mutz and Bensimon (1991), but also genus two geometries, Michalet and Bensimon (1995). Shape transitions in toroidal vesicles have also recently been examined both experimentally and numerically in Noguchi and Imai (2015). Indeed, topology plays a role in almost all intracellular membranes—the Golgi, the Endoplasmic reticulum (rough and smooth alike), as well as the inner membrane of the mitochondrion—exhibit highly nontrivial topologies.

Here we will limit our discussion to an axially symmetric toroidal membrane in order to demonstrate how the topology of a membrane can, itself, provide a source

[23]This is well known in the context of global constraints. In a symmetric closed fluid membrane subject to area and volume constraints, the identity $2\sigma A - 3PV = 0$ is a consequence of the scale invariance of the bending energy, Svetina and Žekž (1989).

of stress in the membrane. Of course, axially symmetric torii have been studied extensively; yet extraordinarily, to our knowledge, never from this more physical point of view. Let the torus have a wheel radius R_0 and tube radius r_0 (see Fig. 3b). Let $\theta = \ell/r_0$ be the angle made along the tube with the outer radial direction, so that $R = R_0 + r_0 \cos\theta$ is the polar radius (the tangent angle is $\Theta = \theta + \pi/2$). The curvature across the tube is constant, $C_\perp = 1/r_0$; whereas that along the wheel is θ dependent: $C_\parallel = \cos\theta/R$. Notice that $C_\perp - C_\parallel = R_0/(r_0 R)$. The Gaussian curvature is positive (negative) on the outer (inner) tube, vanishing on the upper and lower parallels. The mean curvature, K, on the other hand, is positive everywhere unless $2r_0 > R_0$, where it is negative on the interior band of angular width given by $2\theta_0$, where $\cos\theta_0 = -R_0/2r_0$. On a Clifford torus, with $R_0 = \sqrt{2}r_0$, $2\theta_0 = \pi/2$. The sign of K will be reflected in the distribution of stress. Substituting into Eq. (67), one finds that H_{CH} is minimized for a Clifford torus, independent of the physical parameters; the latter do need to be tuned appropriately, Willmore (1965); Ou-Yang (1990); Ou-Yang et al. (1999):

$$P = 2\kappa\, C_0/r_0^2\,, \sigma = \kappa\, C_0(2/r_0 - C_0/2)\,, \tag{95}$$

see also Seifert (1991, 1997). Moreover, the magnitude of the total axial force on a parallel appearing in Eq. (67) is

$$C = -\kappa(1/r_0 + 2C_0)\,. \tag{96}$$

Its origin will be traced to the topology.

In the absence of spontaneous curvature, P and σ vanish and the vertical force is determined by the bending modulus $C = -\kappa/r_0$. Now only the stresses and torques due to bending are relevant. Their nonvanishing projections are given by Eqs. (56) and (80):

$$f_{\perp\perp} = -f_{\parallel\parallel} = \frac{\kappa\, K}{\sqrt{2}\, R}\,, \quad f_\perp = -\frac{\sqrt{2}\kappa}{R^2}\,\sin\theta\,, \tag{97a}$$

$$m_{\perp\parallel} = -\frac{\kappa r_0}{R^2}\left(2\cos^2\theta + \sqrt{2}\cos\theta + 1\right)\,. \tag{97b}$$

$f_{\parallel\parallel}$ correlates directly with mean curvature. It is plotted in Fig. 8a.

Thus the torus is under tension everywhere along the wheel except within the band of angular width $\pi/2$ on the inner tube where K is negative, and tension is replaced by compression. The parallels at $\theta = \pm 3\pi/4$ are free of tangential stress marking the boundary along which tension turns to compression. Because $f_{\perp\perp} = -f_{\parallel\parallel}$, across the tube, tension and compression are interchanged. This behavior, implied by scale invariance is not so intuitively clear.

Topological Torque $\mathbf{M}_\parallel$ *closing the wheel*: The total force closing the tubular cylinder (evaluated, say, on any meridional circle) vanishes, $\mathbf{F}_\parallel = r_0 \int d\theta\, f_{\parallel\parallel}\mathbf{l} = 0$. The moments of the local forces, however, do not vanish. The corresponding torque, closing the torus, is given by $\mathbf{M}_\parallel = 2\pi\kappa\hat{\mathbf{z}}$. It is topological in origin. This behavior contrasts with a cylinder, where the axial force is nonvanishing and there is no torque.

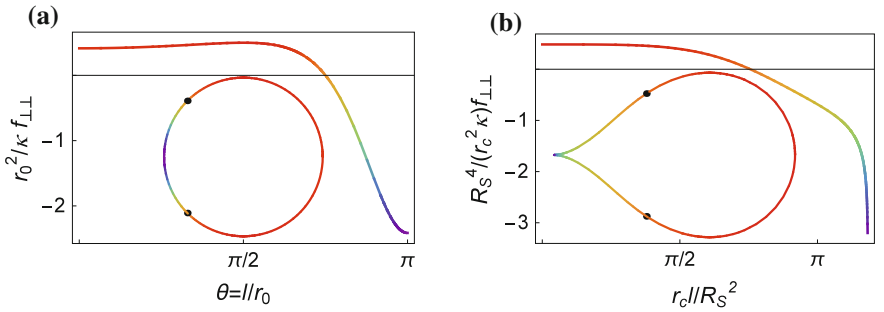

Fig. 8 Components $f_{\perp\perp}$ as function of the arc length l measured from the outer parallel for the **a** Clifford torus **b** discocyte (constructed in Sect. 7). The black dots represent the parallels along which $f_{\perp\perp}$ vanish. Outside of these parallels, the two geometries are essentially indistinguishable; inside the stress diverges in the discocyte reflecting its source in external forces, whereas in the torus it is finite everywhere reflecting its origin in the topology

Topological Force $\mathbf{F}_\perp$ *closing the tube*: The topological force across the tube $\mathbf{F}_\perp$ may be evaluated on any parallel circle (such as the wheel outer circle $\theta = 0$), giving $\mathbf{F}_\perp = \int d\varphi\, R\, (f_{\perp\perp}\mathbf{l} + f_\perp \mathbf{n}) = 2\pi C\, \hat{\mathbf{z}}$. It is also completely determined by the normal forces on appropriate parallels: evaluate $\mathbf{F}_\perp$ along $\theta = \pi/2$.

The corresponding topological torque vanishes, $\mathbf{M}_\perp = 0$. These results quantify the connection between the topology and the internal stresses established in the toroidal membrane. Analogous results will describe higher genus surfaces. But it is not obvious how one would even access this information without knowledge of the local stress and torque in the membrane.

In the next section we will examine some of the consequences of the conformal invariance of bending energy. As we will see, the stress itself is not invariant; and nor are the conserved quantities. And just as well. Under a conformal transformation, an axially symmetric torus will map to a Dupin cyclide, Pinkall (1986). Unlike the energy, which is invariant, the magnitude of the principal stresses increase as the geometry deviates from axial symmetry. As we will describe, the conformally deformed membrane of equal energy may rupture.

7 Conformal Invariance as Probe of Highly Deformed States

An extraordinary feature of the two-dimensional symmetric isotropic bending energy is its invariance under conformal transformations, Willmore (1982, 1996). These are the transformations preserving angles: in addition to its invariance under Euclidean motions it is also scale invariant; less obvious is the fact that it is invariant under inversion in spheres. If this sphere has a radius R_S and is centered at the origin,

inversion is represented by the mapping of points in space: $\mathcal{I} : \mathbf{x} \to \bar{\mathbf{x}} = R_S^2\, \mathbf{x}/|\mathbf{x}|)^2$, where $|\mathbf{x}|^2 := \mathbf{x} \cdot \mathbf{x}$. This induces an inversion of the surface by the replacement of $\mathbf{x}$ by $\mathbf{X}$.

The symmetric bending energy alone rarely provides an accurate description of the physics; typically material fields, constraints, or even a spontaneous curvature will be inconsistent with conformal symmetry. It would be a curiosity were it not for the fact that it can be consistent with nontrivial physically relevant constraints.

Usually one looks at conformal transformations at linear order; let $\mathbf{x} \to \bar{\mathbf{x}} = \mathbf{x} + \delta\mathbf{x}$. Angles are preserved if $d\bar{\mathbf{x}} \cdot d\bar{\mathbf{x}} = \Omega^2(\mathbf{x}) d\mathbf{x} \cdot d\mathbf{x}$. This implies that, correct to linear order, $\delta\mathbf{x}$ satisfies $\partial_i \delta x_j + \partial_j \delta x_i = 2\mathbf{div} \cdot \delta\mathbf{x}\, \delta_{ij}/3$. The most general solution is the sum of a Euclidean motion, a scaling, and a special conformal transformation: $\delta_{\mathbf{c}}\mathbf{x} = |\mathbf{x}|^2\, \mathrm{R}_{\mathbf{x}}\, \delta\mathbf{c}$, where $\mathrm{R}_{\mathbf{x}}$ is the linear operator on three-dimensional space defined by $\mathrm{R}_{\mathbf{x}} = \mathbb{1} - 2\hat{\mathbf{x}} \otimes \hat{\mathbf{x}}$, where $\mathbb{1}$ is the identity transformation and $\hat{\mathbf{x}} = \mathbf{x}/|\mathbf{x}|$; $\mathrm{R}_{\mathbf{x}}$ represents a reflection in the plane perpendicular to $\mathbf{x}$ passing through the origin, so that $\mathrm{R}_{\mathbf{x}}^2 = \mathbb{1}$. The constant space vector $\delta\mathbf{c}$ has dimensions of inverse length squared.

This transformation exponentiates to give (for finite $\mathbf{c}$)

$$\mathbf{x} \to \bar{\mathbf{x}} = \frac{\mathbf{x} + |\mathbf{x}|^2\, \mathbf{c}}{|\mathbf{c}|^2\, |\mathbf{x}|^2 + 2\, \mathbf{c} \cdot \mathbf{x} + 1}\,. \tag{98}$$

This can be recast (we set the radius of inversion equal to one)

$$\bar{\mathbf{x}} = \left(\frac{\mathbf{x}}{|\mathbf{x}|^2} + \mathbf{c}\right) \Big/ \left|\frac{\mathbf{x}}{|\mathbf{x}|^2} + \mathbf{c}\right|^2\,. \tag{99}$$

Thus a finite special conformal transformation can be represented as the composition of an inversion, a translation $\mathbf{c}$, and another inversion: $\mathcal{I}$ o $\mathbf{c}$ o $\mathcal{I}$. Any conformal transformation is a composition of inversions in spheres with Euclidean motions and scalings, Kreyszig (1991). If we understand conformal inversion, we are done.

As was known to the mathematicians of ancient Greece, spheres map to spheres or planes. But, because distances to the center of inversion get inverted, $|\bar{\mathbf{X}}| = R_S^2/|\mathbf{X}|$, points on a sphere will get moved around unless it coincide with the sphere used for inversion. And its center will not remain the center. Other geometries, as we will see, suffer less recognizable distortions.

To understand the conformal symmetry of the bending energy, one needs to know how the two fundamental tensors on a surface transform under inversion. The adapted tangent vectors and the normal vector transform as follows: $\bar{\mathbf{e}}_a \to R_S^2\, \mathrm{R}_{\mathbf{X}}\, \mathbf{e}_a/|\mathbf{X}|^2$, $\mathbf{n} \to -\mathrm{R}_{\mathbf{X}}\, \mathbf{n}$. As a consequence of the former, the induced metric (1) transforms by $g_{ab} \to (R_S/|\mathbf{X}|)^4\, g_{ab}$. Thus in particular, the area measure on the inverted surface is $(R_S/|\mathbf{X}|)^4\, dA$. As for the extrinsic curvature, for our purposes it will suffice to know how the two principal curvatures, C_1, C_2, transform. It follows from the fact that circles map to circles that[24]

[24] $K_{ab} \to K_{ab} = -|\mathbf{X}|^2 \left(K_{ab} - 2\,(\mathbf{X} \cdot \mathbf{n}) g_{ab}/|\mathbf{X}|^{-2}\right)$.

$$C_I \to -(|\mathbf{X}|/R_S)^2 \left(C_I - 2\,\mathbf{X}\cdot\mathbf{n}/|\mathbf{X}|^2\right)\,,\; I = 1, 2; \tag{100}$$

their difference thus transforms multiplicatively, or

$$C_1 - C_2 \to -(|\mathbf{X}|/R_S)^2\,(C_1 - C_2)\,. \tag{101}$$

This result, together with the transformation of area, implies that the energy

$$H_W = \frac{1}{2}\int dA\,(C_1 - C_2)^2 \tag{102}$$

is manifestly invariant. It follows that the unadorned quadratic bending energy, $H_B = \kappa/2\int dA\,(C_1 + C_2)^2 + \bar{\kappa}\int dA\,C_1C_2$ is also invariant—unless the topology changes.

Two physically significant consequences are immediate:
(1) any two geometries related by a conformal transformation possess the same bending energy if the topology is unchanged.
(2) if one of these geometries is an equilibrium state of this energy, then the other is also, modulo possible pointlike singularities. We will show that these singularities can be interpreted as external forces acting on the membrane.

In the 90s Seifert and coworkers, Seifert (1991); Jülicher et al. (1993); Jülicher (1996), observed a degeneracy in the ground states of higher genus vesicles, which they dubbed conformal diffusion, associated with the existence of conformal transformations preserving constraints. This involved examining the behavior of the constrained energy under small special conformal transformations. Such transformations induce continuous deformations of the surface. We will focus on conformal inversion, a non-perturbative feature of conformal symmetry that cannot be probed by exponentiation. It will provide a window, albeit a narrow one of its choosing, into the non-perturbative response of membranes to external forces.

Suppose that the geometry we begin with is not compact. Its image under inversion generally will be compact. To illustrate this point, let us examine the inversion of a catenoid, a minimal surface. The catenoid is described in polar coordinates by $R(Z) = r_0\,\cosh(Z/r_0)$, where r_0 here is its neck radius. Under an inversion centered at the origin, this catenoid maps into the axisymmetric geometry with radial and height coordinates,

$$\bar{R}(Z) = R_S^2 R(Z)/(R(Z)^2 + Z^2)\,;\quad \bar{Z}(Z) = R_S^2\,Z/(R(Z)^2 + Z^2)\,,\, -\infty < Z < \infty\,. \tag{103}$$

Its image resembles a discocyte (see Fig. 9), but this coincidence should not be taken too literally: there are many physical mechanisms producing superficially identical morphologies.[25] While the catenoid and its inverted image are linked mathematically, they are topologically different and clearly describe very different physics, Castro-Villarreal and Guven (2007a, b). Whereas the catenoid is well known, the second

[25] Fixing the discocyte area at $4\pi r_0^2$ determines $R_S = 1.089\,r_0$.

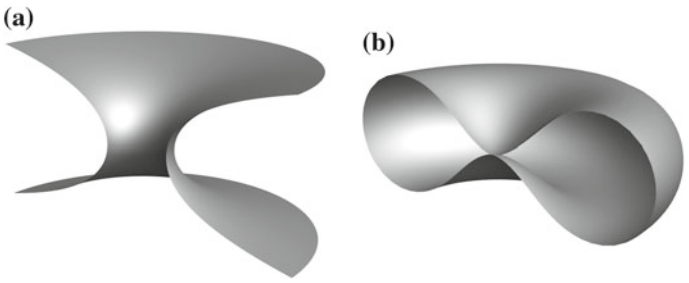

Fig. 9 **a** Catenoid and **b** discocyte obtained by its inversion in a sphere centered at the origin

geometry is not and, had it not been for the stratagem provided by inversion, it is unlikely that one would have guessed that this simple discocyte describes an equilibrium, nevermind lending itself to an exact analytical treatment.

Let us examine the discocyte geometry more closely. Under inversion, the two ends of the catenoid map to the origin, forming the north and south poles of the discocyte which touch with a common tangent plane. The existence of a tangent plane, however, belies the fact that curvature singularities are present at these points: the source-free EL equation breaks down implying the presence of localized distributional external forces. The mathematical origin of these singularities is the compactification of the exponential ends into a bounded region, Castro-Villarreal and Guven (2007a, b); Guven and Vázquez-Montejo (2013b). Note that, in contrast with a catenoid, the inversion of a hyperboloid of revolution—which is asymptotically conical—gives a pair of conical singularity at the origin, without tangent planes to hide behind. We will have more to say about singularities in a moment. Notice also that whereas $\int dA\, C_1 C_2 = -4\pi$ for a catenoid, it is given by 4π for a discocyte, which is topologically a sphere. That the poles touch is irrelevant.

Whereas the distribution of stress associated with bending vanishes in a catenoid, it does not in the discocyte. The tangential stress along the meridian $f_{\perp\perp} = -f_{\parallel\parallel}$ is plotted in Fig. 8b as a functions of archlength, l, measured from the outer parallel. It is observed that it is strongly localized within the neighborhoods of the two touching poles, where it diverges.

If we now translate the center of inversion along the axis of the catenoid, a one-parameter family of equilibrium states is generated: as illustrated for a northward movement in Fig. 10, the symmetric discocyte morphs smoothly into a stomatocyte. The limiting shape is a sphere within a sphere, touching at the bottom, connected by a microscopic catenoidal neck at the top. Unlike the constricted sphere discussed previously, this time the neck is a catenoid because there are no sources acting within it.

Now let us place the center of inversion off axis, Guven and Vázquez-Montejo (2013b). Consider, for example, inversion in a sphere centered on a point located

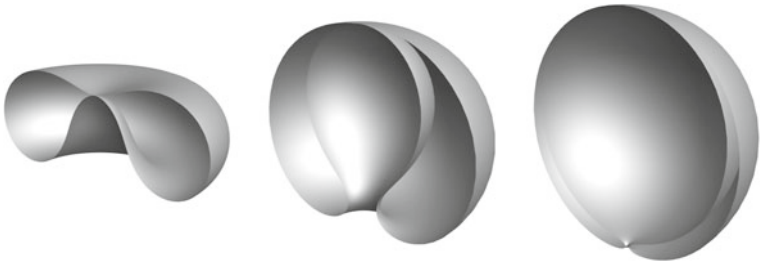

(a) $z_0 = 1$ b) $z_0 = 10$ (c) $z_0 = 100$

Fig. 10 Surfaces generated by inversion of a catenoid in spheres centered at height z_0 along its axis of symmetry

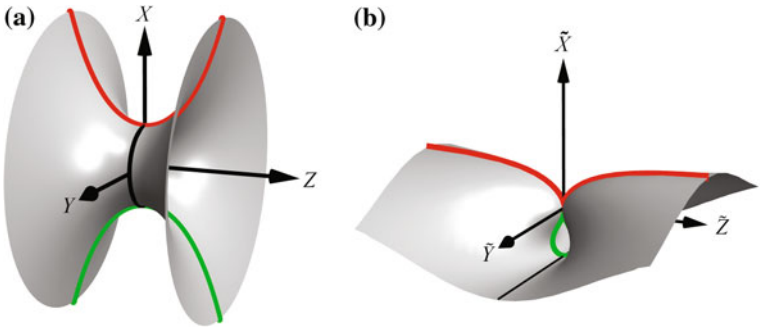

Fig. 11 The *red* and *green* catenaries on the mirror plane $Y = 0$ map to a single curve. The circular neck maps to a straight line

along the X axis. This preserves the mirror symmetries in the XZ and XY planes.[26] In Fig. 12, we illustrate four geometries in this sequence. Of special interest are those generated when this point lies close to the neck of the catenoidal geometry, say $\mathbf{x}_0 = (1 + \epsilon) r_0 \mathbf{i}$, with ϵ small. Now, the neighborhood of the point $r_0\mathbf{i}$ on the neck gets inflated into a large spherical region: the geometry is spherical almost everywhere, with a *defect*, formed by the two points held together, localized upon it as indicated in Fig. 12b, c.

To facilitate the visualization of this construction, it is useful to follow the fate of the catenary meridians and the neck of the catenoid as illustrated in Fig. 11.

Physically, one can interpret these geometries as the end point of a procedure bringing two nearby points on an almost spherical vesicle, of fixed area and fixed enclosed volume, into contact by applying normal forces (as opposed to tangential ones which would not disturb the initial geometry, fluid in its tangent plane), Guven

[26]The bilateral symmetry (not necessarily in the original XZ plane) is preserved if the point strays off this axis; however, the up-down symmetry is broken, just as it was in the axially symmetric family.

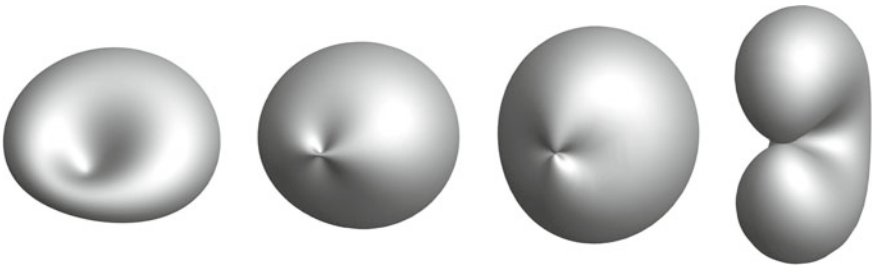

(a) $x_0 = 0.5$ (b) $x_0 = 0.93$ (c) $x_0 = 1.07$ (d) $x_0 = 2$

Fig. 12 Surfaces generated by inversion of a catenoid in a sphere centered at increasing distances along the radial direction

and Vázquez-Montejo (2013b). Conformal invariance may grant access to the non-pertubative equilibrium end state, but it does not have anything to say about the intermediate states—with the two points still separated—through which the membrane has to pass on its way to this final state. As we have pointed out, conformal invariance decides what window it opens.

If $\epsilon < 0$, the geometry represents two nearby points on the vesicle that are pinched together; it resembles the wrinkle forming on skin that has been pinched. If $\epsilon > 0$, on the other hand, two fingers of membrane—touching at a point—project out from the vesicle. In the latter the force is directed out of the vesicle, not into it as in the former. Despite the apparent differences in the two descriptions, however, it takes only a moment's thought to appreciate that the two limiting geometries are mirror images in the neighborhood of the defect.

These geometries are also stable. The constraints on the area and on the volume reduce the conformal symmetry to a single nontrivial degree of freedom. This is reflected in a zero mode of the operator controlling fluctuations corresponding to deformations which break the up-down mirror symmetry in the XY plane but leave fixed the geodesic distance s along the surface separating the two touching points.[27] As a consequence, once formed, the membrane cannot slip out of this defect. If the volume constraint were to be relaxed, however, there would be nothing to prevent the two points from approaching each other along the membrane.

More exotic increasingly deflated geometries are generated by increasing the magnitude of $\mathbf{x}_0$. The surface first morphs continuously into a folded sausage, as illustrated in Fig. 12d; beyond a critical value of x_0, the waist on the sausage begins to constrict. As x_0 increases further, the geometry evolves, just like its axially symmetry counterpart, into a geometry that is spherical almost everywhere: this time it resembles two spherical lobes, touching at one point and connected by a vanishingly small catenoidal neck adjacent to it.

[27] This is the shortest distance between the two points on the surface. They are, of course, in contact in space.

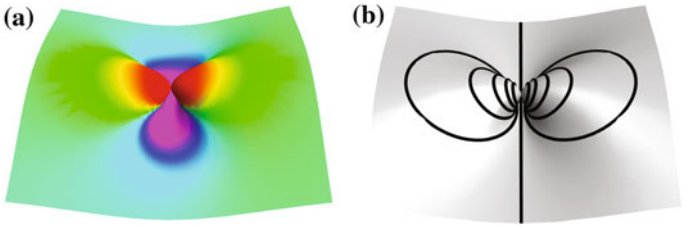

Fig. 13 **a** Stress across the images of parallel circles. **b** Images of parallel circles represented by closed curves

On a catenoid, $\mathbf{f}^a = 0$. In the inverted geometry, $K \neq 0$ and equilibrium involves a nontrivial balance of normal and tangential stresses. These stresses possess a pair of external sources ($\pm\mathbf{F}$ say) normal to the surface localized at the points of contact; this is what holds them together. It is easy to show that in the height function description of the geometry with respect to the local tangent plane at these points, one has $h \approx \mp r^2 \ln r$, where r is the polar radius.[28,29] The presence of a source is signaled geometrically by the logarithmic curvature singularity at these points.

To identify the contact force $\mathbf{F}$, we can deform the contour surrounding the pole so that it coincide with the line of symmetry running along the valley (or ridge) between the two poles. Using the expression for the force given in Eq. (77), one determines $\mathbf{F} \approx 9.65\pi\kappa/s\,\mathbf{k}$. Note that the detailed distribution of stress is not required to determine the contact force, Guven and Vázquez-Montejo (2013b). As the vesicle is inflated, s decreases and the contact force increases. One can show, however, that it remains below the rupture tension of the membrane until $s \approx 20\,\text{nm}$, a separation so small that the mesoscopic modeling in terms of a surface is no longer reliable (Fig. 13).

There is also an important cautionary point to be emphasized here: had one used the Monge representation for the horizontal stress with respect to the local tangent plane, an incorrect answer would have been obtained.

---

[28] An unexpected duality between the weak field behavior in one geometry and the strong field behavior in the other is evident: asymptotically, the catenoid is accurately described by the height function $h \sim \ln r$, $r \gg r_0$; this asymptotic region is mapped into the neighborhood of the poles described by $h \sim -r^2 \ln r$, $r \ll s$. Inversion provides a connection between the harmonic behavior in the former and the biharmonic behavior in the latter, Guven and Vázquez-Montejo (2013b). To understand this duality between harmonic and biharmonic function, look at the inversion in the origin $\mathbf{x} \to \mathbf{x}/|\mathbf{x}|^2$ (for transparency set the scale to one), described in the height function representation by $(r, h) \to (r, h)/((r^2 + h^2)$, so that $h \approx \ln r \to \frac{h}{r^2+h^2} = \ln[r/(r^2 + h^2)]$. Now, if $h \ll r$, then $\frac{h}{r^2} \approx -\ln r$, and as claimed the Green function of the Laplacian is mapped to its biharmonic counterpart.

[29] In this context, note also that the symmetric saddle with $h \sim r^2 \cos 2\theta$ maps to the biharmonic dipole $h \sim \cos 2\theta$.

8 Concluding Remarks

Despite the complexity of the cellular environment on the molecular scale, on zooming out, one finds that much of the equilibrium physics of cellular membranes on mesoscopic scales can be understood by treating the membrane as a two-dimensional surface described by an energy depending only on its geometry. This implies that this physics is completely encoded in the membrane geometry. We have presented a number of simple examples to illustrate the nature of this connection. Even if additional structure is relevant, it can be treated in terms of fields interacting with this geometry.

There are other examples falling within the scope of this chapter which we have not treated for want of space, or because they will be treated thoroughly by other contributors. Some of these are treated, as commented previously, in a nice recent review, Deserno (2015). Here this framework is used to determine the Gaussian bending modulus of a buckled membrane. The interested reader can find a statistical mechanical treatment of the stress tensor, important but absent in our presentation, in Shiba et al. (2016). Membranes in a viscous fluid are examined by Powers (2010), membrane viscosity itself is accommodated in Arroyo and DeSimone (2009).

To explore how confinement can shape a membrane, Müller and his coworkers have looked at the confinement of a topologically spherical membrane within another membrane of smaller area, Kahraman et al. (2012a, b). This can be thought of as a model of the inner membrane of the mitochondrion, capturing the geometrical aspect of the physics. As the area is increased, in addition to the external forces associated with confinement, self-contacts will occur breaking the symmetry of the ground state. If membrane fusion occurs, the topology will change accompanied by a large scale reorganization of the ground state geometry, Bouzar et al. (2015).

Deflated high-genus geometries are exhibited by the nuclear envelope and the Golgi apparatus. In the limit where the enclosed volume becomes very small, in the absence of additional agents, the ground state of a closed fluid membrane with a fixed genus g approximates two concentric spherical bilayers connected by $g + 1$ catenoidal necks (Kusner and Yu, private communication). Recent simulations, involving additional players with their own degrees of freedom, controlling the pore radius provide a more accurate description of the nuclear envelope, Noguchi (2016a). In this context, the stability of the inner ramp boundaries in the rough ER described in Sect. 4. appears to involve the condensation along their length of membrane-shaping proteins, Guven et al. (2014); Schweitzer and Kozlov (2015); Noguchi (2016b). While getting the biological details right always involves elaborate numerical analysis; understanding how the membrane geometry gets shaped by external forces and constraints will inform how we go about it.

Acknowledgements JG would like to thank David Steigmann for the invitation to lecture at the CISM Summer School held in Udine, Italy during July of 2016. This chapter is based on these lectures. We would like also to thank Markus Deserno, Martin Müller and Saša Svetina for their valuable input. This work was partially supported by CONACyT grant 180901.

References

L. Amoasii, K. Hnia, G. Chicanne, A. Brech, B.S. Cowling, M.M. Müller, Y. Schwab, P. Koebel, A. Ferry, B. Payrastre, J. Laporte, Myotubularin and ptdins3p remodel the sarcoplasmic reticulum in muscle in vivo. J. Cell Sci. **126**(8), 1806–1819 (2013). doi:10.1242/jcs.118505

R. Arnowitt, S. Deser, C.W. Misner, Dynamical structure and definition of energy in general relativity. Phys. Rev. **116**(5), 1322–1330 (1959). doi:10.1103/PhysRev.116.1322

G. Arreaga, R. Capovilla, J. Guven, Noether currents for bosonic branes. Ann. Phys. **279**(1), 126–158 (2000). doi:10.1006/aphy.1999.5979

M. Arroyo, A. DeSimone, Relaxation dynamics of fluid membranes. Phys. Rev. E **79**(3), 031915 (2009). doi:10.1103/PhysRevE.79.031915

P. Bassereau, B. Sorre, A. Lévy, Bending lipid membranes: experiments after w. helfrich's model. Adv. Colloid Interface Sci. **208**, 47–57 (2014). doi:10.1016/j.cis.2014.02.002. Special issue in honour of Wolfgang Helfrich

Y. Bernard, Noether's theorem and the willmore functional. Adv. Calc. Var. (2015). doi:10.1515/acv-2014-0033

L. Bouzar, F. Menas, M.M. Müller, Toroidal membrane vesicles in spherical confinement. Phys. Rev. E **92**, 032721 (2015). doi:10.1103/PhysRevE.92.032721

B. Božič, J. Guven, P. Vázquez-Montejo, S. Svetina, Direct and remote constriction of membrane necks. Phys. Rev. E **89**, 052701 (2014). doi:10.1103/PhysRevE.89.052701

B. Božič, S.L. Das, S. Svetina, Sorting of integral membrane proteins mediated by curvature-dependent protein-lipid bilayer interaction. Soft Matter **11**, 2479–2487 (2015). doi:10.1039/C4SM02289K

P.B. Canham, The minimum energy of bending as a possible explanation of the biconcave shape of the human red blood cell. J. Theor. Biol. **26**(1), 61–81 (1970). doi:10.1016/S0022-5193(70)80032-7

R. Capovilla, J. Guven, Geometry of lipid vesicle adhesion. Phys. Rev. E **66**, 041604 (2002a). doi:10.1103/PhysRevE.66.041604

R. Capovilla, J. Guven, Stresses in lipid membranes. J. Phys. A Math. Gen. **35**(30), 6233 (2002b). doi:10.1088/0305-4470/35/30/302

R. Capovilla, J. Guven, Stress and geometry of lipid vesicles. J. Phys.-Condens. Mat. **16**, S2187–S2191 (2004a). doi:10.1088/0953-8984/16/22/018

R. Capovilla, J. Guven, Second variation of the Helfrich-Canham Hamiltonian and reparametrization invariance. J. Phys. A Math. Gen. **37**(23), 5983 (2004b). doi:10.1088/0305-4470/37/23/003

R. Capovilla, J. Guven, J.A. Santiago, Lipid membranes with an edge. Phys. Rev. E **66**, 021607 (2002). doi:10.1103/PhysRevE.66.021607

R. Capovilla, J. Guven, J.A. Santiago, Deformations of the geometry of lipid vesicles. J. Phys. A Math. Gen. **36**(23), 6281 (2003). doi:10.1088/0305-4470/36/23/301

P. Castro-Villarreal, J. Guven, Axially symmetric membranes with polar tethers. J. Phys. A Math. Theor. **40**(16), 4273 (2007a). doi:10.1088/1751-8113/40/16/002

P. Castro-Villarreal, J. Guven, Inverted catenoid as a fluid membrane with two points pulled together. Phys. Rev. E **76**, 011922 (2007b). doi:10.1103/PhysRevE.76.011922

M. Deserno, Membrane elasticity and mediated interactions in continuum theory: a differential geometric approach, in *Biomembrane Frontiers*, ed. by R. Faller, M.L. Longo, S.H. Risbud, T. Jue. Handbook of Modern Biophysics (Humana Press, New York, 2009), pp. 41–74. doi:10.1007/978-1-60761-314-5_2

M. Deserno, Fluid lipid membranes: from differential geometry to curvature stresses. Chem. Phys. Lipids **185**, 11–45 (2015). doi:10.1016/j.chemphyslip.2014.05.001. Membrane mechanochemistry: From the molecular to the cellular scale

M. Deserno, M.M. Müller, J. Guven, Contact lines for fluid surface adhesion. Phys. Rev. E **76**, 011605 (2007). doi:10.1103/PhysRevE.76.011605

P. Diggins IV, Z.A. McDargh, M. Deserno, Curvature softening and negative compressibility of gel-phase lipid membranes. J. Am. Chem. Soc. **137**(40), 12752–12755 (2015). doi:10.1021/jacs.5b06800

M. Do Carmo, *Differential Geometry of Curves and Surface* (Prentice Hall, Upper Saddle River, 1976)

M. Do Carmo. *Riemannian Geometry*. (Birkhauser, Basel, 1992)

P.G. Dommersnes, J.-B. Fournier, The many-body problem for anisotropic membrane inclusions and the self-assembly of saddle defects into an egg carton. Biophys. J. **83**, 2898–2905 (2002). doi:10.1016/S0006-3495(02)75299-5

E.A. Evans, Bending resistance and chemically induced moments in membrane bilayers. Biophys. J. **14**, 923–931 (1974). doi:10.1016/S0006-3495(74)85959-X

E.A. Evans, R. Skalak, *Mechanics and Thermodynamics of Biomembranes* (CRC Press, Boca Raton, 1980)

J.-B. Fournier, On the stress and torque tensors in fluid membranes. Soft Matter **3**, 883–888 (2007). doi:10.1039/B701952A

J.-B. Fournier, Dynamics of the force exchanged between membrane inclusions. Phys. Rev. Lett. **112**, 128101 (2014). doi:10.1103/PhysRevLett.112.128101

J.-B. Fournier, P. Galatola, High-order power series expansion of the elastic interaction between conical membrane inclusions. Eur. Phys. J. E **38**(8) (2015). doi:10.1140/epje/i2015-15086-3

R. Goetz, W. Helfrich, The egg carton: theory of a periodic superstructure of some lipid membranes. J. Phys. II Fr. **6**(2), 215–223 (1996). doi:10.1051/jp2:1996178

M. Goulian, R. Bruinsma, P. Pincus, Long-range forces in heterogeneous fluid membranes. EPL (Europhysics Letters) **22**(2), 145 (1993). doi:10.1209/0295-5075/22/2/012

J. Guven, Membrane geometry with auxiliary variables and quadratic constraints. J. Phys. A Math. Gen. **37**(28), L313 (2004). doi:10.1088/0305-4470/37/28/L02

J. Guven, Conformally invariant bending energy for hypersurfaces. J. Phys. A Math. Gen. **38**(37), 7943 (2005). doi:10.1088/0305-4470/38/37/002

J. Guven, Laplace pressure as a surface stress in fluid vesicles. J. Phys. A Math. Gen. **39**(14), 3771 (2006). doi:10.1088/0305-4470/39/14/019

J. Guven, M.M. Müller, How paper folds: bending with local constraints. J. Phys. A Math. Theo. **41**(5), 055203 (2008). doi:10.1088/1751-8113/41/5/055203

J. Guven, M.M. Müller, P. Vázquez-Montejo, Conical instabilities on paper. J. Phys. A Math. Theo. **45**(1), 015203 (2012). doi:10.1088/1751-8113

J. Guven, P. Vázquez-Montejo, Spinor representation of surfaces and complex stresses on membranes and interfaces. Phys. Rev. E **82**, 041604 (2010). doi:10.1103/PhysRevE.82.041604

J. Guven, P. Vázquez-Montejo, Constrained metric variations and emergent equilibrium surfaces. Phys. Lett. A **377**(23–24), 1507–1511 (2013a). doi:10.1016/j.physleta.2013.04.031

J. Guven, P. Vázquez-Montejo, Force dipoles and stable local defects on fluid vesicles. Phys. Rev. E **87**, 042710 (2013b). doi:10.1103/PhysRevE.87.042710

J. Guven, G. Huber, D.M. Valencia, Terasaki spiral ramps in the rough endoplasmic reticulum. Phys. Rev. Lett. **113**, 188101 (2014). doi:10.1103/PhysRevLett.113.188101

R.C. Haussman, M. Deserno, Effective field theory of thermal casimir interactions between anisotropic particles. Phys. Rev. E **89**, 062102 (2014). doi:10.1103/PhysRevE.89.062102

W. Helfrich, Elastic properties of lipid bilayers, theory and possible experiments. Z. Naturforsch. C **28**, 693–703 (1973). http://zfn.mpdl.mpg.de/data/Reihe_C/28/ZNC-1973-28c-0693.pdf

J.H. Jellett. Sur la surface dont la courbure moyenne est constante. Journal de Mathematiques Pures et Appliquees, 163–167 (1853)

J.T. Jenkins, The equations of mechanical equilibrium of a model membrane. SIAM J. Appl. Math. **32**(4), 755–764 (1977). doi:10.1137/0132063

F. Jülicher, The morphology of vesicles of higher topological genus: conformal degeneracy and conformal modes. J. Phys. II Fr. **6**(12), 1797–1824 (1996). doi:10.1051/jp2:1996161

F. Jülicher, U. Seifert, Shape equations for axisymmetric vesicles: a clarification. Phys. Rev. E **49**, 4728–4731 (1994). doi:10.1103/PhysRevE.49.4728

F. Jülicher, U. Seifert, R. Lipowsky, Conformal degeneracy and conformal diffusion of vesicles. Phys. Rev. Lett. **71**, 452–455 (1993). doi:10.1103/PhysRevLett.71.452
O. Kahraman, N. Stoop, M.M. Müller, Morphogenesis of membrane invaginations in spherical confinement. EPL (Europhysics Letters) **97**(6), 68008 (2012a). doi:10.1209/0295-5075/97/68008
O. Kahraman, N. Stoop, M.M. Müller, Fluid membrane vesicles in confinement. New J. Phys. **14**(9), 095021 (2012b). doi:10.1088/1367-2630/14/9/095021
K.S. Kim, J. Neu, G. Oster, Curvature-mediated interactions between membrane proteins. Biophys. J. **75**(5), 2274–2291 (1998). doi:10.1016/S0006-3495(98)77672-6
M.M. Kozlov, Fission of biological membranes: interplay between dynamin and lipids. Traffic **2**(1), 51–65 (2001). doi:10.1034/j.1600-0854.2001.020107.x
V. Kralj-Iglič, S. Svetina, B. Žekž, Shapes of bilayer vesicles with membrane embedded molecules. Eur. Biophys. J. **24**(5), 311–321 (1996). doi:10.1007/BF00180372
V. Kralj-Iglič, V. Heinrich, S. Svetina, B. Žekž, Free energy of closed membrane with anisotropic inclusions. Eur. Phys. J. B - Condens. Matter Complex Syst. **10**(1), 5–8 (1999). doi:10.1007/s100510050822
E. Kreyszig, *Differential Geometry* (Dover Publications, New York, 1991)
R. Kusner, Geometric analysis and computer graphics, in *Mathematical Sciences Research Institute Publications*, vol. 17, ed. by P. Concus, R. Finn, D.A. Hoffman (Springer, New York, 1991), pp. 103–108. doi:10.1007/978-1-4613-9711-3_11
R. Lipowsky, Spontaneous tubulation of membranes and vesicles reveals membrane tension generated by spontaneous curvature. Faraday Discuss. **161**, 305–331 (2013). doi:10.1039/C2FD20105D
M.A. Lomholt, L. Miao, Descriptions of membrane mechanics from microscopic and effective two-dimensional perspectives. J. Phys. A Math. Gen. **39**(33), 10323 (2006). doi:10.1088/0305-4470/39/33/005
O.V. Manyuhina, J.J. Hetzel, M.I. Katsnelson, A. Fasolino, Non-spherical shapes of capsules within a fourth-order curvature model. Eur. Phys. J. E **32**(3), 223–228 (2010). doi:10.1140/epje/i2010-10631-2
F.C. Marques, A. Neves, Min-Max theory and the Willmore conjecture. Ann. Math. Second Series **179**(2), 683–782 (2014a). doi:10.4007/annals.2014.179.2.6
F.C. Marques, A. Neves, The Willmore conjecture. Jahresbericht der Deutschen Mathematiker-Vereinigung **116**(4), 201–222 (2014b). doi:10.1365/s13291-014-0104-8
Z. McDargh, P. Vázquez-Montejo, J. Guven, M. Deserno. Constriction by dynamin: Elasticity vs. adhesion. Biophy. J. **111**(11), 2470–2480 (2016). doi:10.1016/j.bpj.2016.10.019
X. Michalet, D. Bensimon, Observation of stable shapes and conformal diffusion in genus 2 vesicles. Science **269**(5224), 666–668 (1995). doi:10.1126/science.269.5224.666
S. Morlot, A. Roux, Mechanics of dynamin-mediated membrane fission. Ann. Rev. Biophys. **42**(1), 629–649 (2013). doi:10.1146/annurev-biophys-050511-102247
M.M. Müller, Theoretical studies of fluid membrane mechanics, Ph.D. thesis, University of Mainz (Germany), 2007
M.M. Müller, M. Deserno, J. Guven, Geometry of surface-mediated interactions. Europhys. Lett. **69**(3), 482 (2005a). doi:10.1209/epl/i2004-10368-1
M.M. Müller, M. Deserno, J. Guven, Interface-mediated interactions between particles: a geometrical approach. Phys. Rev. E **72**, 061407 (2005b). doi:10.1103/PhysRevE.72.061407
M.M. Müller, M. Deserno, J. Guven, Balancing torques in membrane-mediated interactions: exact results and numerical illustrations. Phys. Rev. E **76**, 011921 (2007). doi:10.1103/PhysRevE.76.011921
M. Mutz, D. Bensimon, Observation of toroidal vesicles. Phys. Rev. A **43**, 4525–4527 (1991). doi:10.1103/PhysRevA.43.4525
G.-M. Nam, N.-K. Lee, H. Mohrbach, A. Johner, I.M. Kulić, Helices at interfaces. EPL (Europhysics Letters) **100**(2), 28001 (2012). doi:10.1209/0295-5075/100/28001
H. Noguchi, Construction of nuclear envelope shape by a high-genus vesicle with pore-size constraint. Biophy. J. **111**(4), 824–831 (2016a). doi:10.1016/j.bpj.2016.07.010

H. Noguchi, Membrane tubule formation by banana-shaped proteins with or without transient network structur. Sci. Rep. **6**, 20935 (2016b). doi:10.1038/srep20935
A.S.H. Noguchi, M. Imai, Shape transformations of toroidal vesicles. Soft Matter **11**, 193–201 (2015)
Z.-C. Ou-Yang, Anchor ring-vesicle membranes. Phys. Rev. A **41**, 4517–4520 (1990). doi:10.1103/PhysRevA.41.4517
Z.-C. Ou-Yang, W. Helfrich, Instability and deformation of a spherical vesicle by pressure. Phys. Rev. Lett. **59**, 2486–2488 (1987). doi:10.1103/PhysRevLett.59.2486
Z.-C. Ou-Yang, W. Helfrich, Bending energy of vesicle membranes: General expressions for the first, second, and third variation of the shape energy and applications to spheres and cylinders. Phys. Rev. A **39**, 5280–5288 (1989). doi:10.1103/PhysRevA.39.5280
Z.C. Ou-Yang, J.X. Liu, Y.Z. Xie, X. Yu-Zhang, *Geometric Methods in the Elastic Theory of Membranes in Liquid Crystal Phases, Advanced series on theoretical physical science* (World Scientific, Singapore, 1999)
R. Phillips, T. Ursell, P. Wiggins, P. Sens, Emerging roles for lipids in shaping membrane-protein function. Nature **459**, 379–385 (2009). doi:10.1038/nature08147
U. Pinkall, Cyclides of Dupin, in *Mathematical Models from the Collections of Universities and Museums*, ed. by E.G. Fischer. Advanced Lectures in Mathematics Series (Friedrick Vieweg & Son, Braunschweig, 1986), pp. 28–30. Chap. 3.3
R. Podgornik, S. Svetina, B. Žekš, Parametrization invariance and shape equations of elastic axisymmetric vesicles. Phys. Rev. E **51**, 544–547 (1995). doi:10.1103/PhysRevE.51.544
T.R. Powers, Dynamics of filaments and membranes in a viscous fluid. Rev. Mod. Phy. **82**(2), 1607–1631 (2010). doi:10.1103/RevMod-Phys.82.1607
B.J. Reynwar, G. Illya, V.A. Harmandaris, M.M. Müller, K. Kremer, M. Deserno, Aggregation and vesiculation of membrane proteins by curvature-mediated interactions. Nature **447**, 461–464 (2007). doi:10.1038/nature05840
Y. Schweitzer, M. Kozlov, Membrane-mediated interaction between strongly anisotropic protein scaffolds. PLoS Comput. Biol. **11**, 1004054 (2015). doi:10.1371/journal.pcbi.1004054
U. Seifert, Conformal transformations of vesicle shapes. J. Phys. A Math. Gen. **24**(11), 573 (1991). doi:10.1088/0305-4470/24/11/001
U. Seifert, Vesicles of toroidal topology. Phys. Rev. Lett. **66**, 2404–2407 (1991). doi:10.1103/PhysRevLett.66.2404
U. Seifert, Configurations of fluid membranes and vesicles. Adv. Phys. **46**(1), 13–137 (1997). doi:10.1080/00018739700101488
U. Seifert, R. Lipowsky, Morphology of vesicles, in *Structure and Dynamics of Membranes From Cells to Vesicles*, ed. by R. Lipowsky, E. Sackmann. Handbook of Biological Physics, vol. 1 (North-Holland, Amsterdam, 1995), pp. 403–463. doi:10.1016/S1383-8121(06)80025-4
P. Sens, L. Johannes, P. Bassereau, Biophysical approaches to protein-induced membrane deformations in trafficking. Current Opinion Cell Biol. **20**(4), 476–482 (2008). doi:10.1016/j.ceb.2008.04.004
H. Shiba, H. Noguchi, J.-B. Fournier, Monte carlo study of the frame, fluctuation and internal tensions of fluctuating membranes with fixed area. Soft Matter **12**, 2373–2380 (2016). doi:10.1039/C5SM01900A
M. Spivak, *A Comprehensive Introduction to Differential Geometry*, vol. 1–5, 3rd edn. (Publish or Perish, Inc., Houston, 1999)
D.J. Steigmann, Fluid films with curvature elasticity. Arch. Rational Mech. Anal. **150**(2), 127–152 (1999). doi:10.1007/s002050050183
S. Svetina, B. Žekž, Membrane bending energy and shape determination of phospholipid vesicles and red blood cells. Eur. Biophys. J. **17**(2), 101–111 (1989). doi:10.1007/BF00257107
S. Svetina, B. Žekš, Nonlocal membrane bending: a reflection, the facts and its relevance. Adv. Colloid Interface Sci. **208**, 189–196 (2014). doi:10.1016/j.cis.2014.01.010. Special issue in honour of Wolfgang Helfrich

M. Terasaki, T. Shemesh, N. Kasthuri, R.W. Klemm, R. Schalek, K.J. Hayworth, A.R. Hand, M. Yankova, G. Huber, J.W. Lichtman, T.A. Rapoport, M.M. Kozlov, Stacked endoplasmic reticulum sheets are connected by helicoidal membrane motifs. Cell **154**, 285–296 (2013). doi:10.1016/j.cell.2013.06.031

Z.C. Tu, Z.C. Ou-Yang, Lipid membranes with free edges. Phys. Rev. E **68**, 061915 (2003). doi:10.1103/PhysRevE.68.061915

Z.C. Tu, Z.C. Ou-Yang, A geometric theory on the elasticity of bio-membranes. J. Phys. A Math. Gen. **37**(47), 11407 (2004). doi:10.1088/0305-4470/37/47/010

Z.C. Tu, Z.C. Ou-Yang, Recent theoretical advances in elasticity of membranes following helfrich's spontaneous curvature model. Adv. Colloid Interface Sci. **208**, 66–75 (2014). doi:10.1016/j.cis.2014.01.008. Special issue in honour of Wolfgang Helfrich

R.M. Wald, *General Relativity* (University of Chicago Press, Chicago, 2010)

T.R. Weikl, M.M. Kozlov, W. Helfrich, Interaction of conical membrane inclusions: effect of lateral tension. Phys. Rev. E **57**, 6988–6995 (1998). doi:10.1103/PhysRevE.57.6988

T.J. Willmore, Note on embedded surfaces. An. St. Univ. Iasi, sIa Mat. B **12**, 493–496 (1965)

T.J. Willmore, *Total Curvature in Riemannian Geometry* (Ellis Horwood, Chichester, 1982)

T.J. Willmore, *Riemannian Geometry* (Oxford University Press, Oxford, 1996)

C. Yolcu, M. Deserno, Membrane-mediated interactions between rigid inclusions: an effective field theory. Phys. Rev. E **86**, 031906 (2012). doi:10.1103/PhysRevE.86.031906

C. Yolcu, I.Z. Rothstein, M. Deserno, Effective field theory approach to casimir interactions on soft matter surfaces. EPL (Europhysics Letters) **96**(2), 20003 (2011). doi:10.1209/0295-5075/96/20003

C. Yolcu, I.Z. Rothstein, M. Deserno, Effective field theory approach to fluctuation-induced forces between colloids at an interface. Phys. Rev. E **85**, 011140 (2012). doi:10.1103/PhysRevE.85.011140

C. Yolcu, R.C. Haussman, M. Deserno, The effective field theory approach towards membrane-mediated interactions between particles. Adv. Colloid Interface Sci. **208**, 89–109 (2014). doi:10.1016/j.cis.2014.02.017. Special issue in honour of Wolfgang Helfrich

W.-M. Zheng, J. Liu, Helfrich shape equation for axisymmetric vesicles as a first integral. Phys. Rev. E **48**, 2856–2860 (1993). doi:10.1103/PhysRevE.48.2856